Geotech Geol Eng (2025) 43:58
https://doi.org/10.1007/s10706-024-03002-0

ORIGINAL PAPER

Performance of Confined Concrete-Filled Aluminum Tube Pile Groups under Combined Loading

Fadhil Al-Darraji · Monower Sadique · Zelong Yu · Ali Shubbar · Tina Marolt Čebašek

Received: 16 May 2024 / Accepted: 22 October 2024

Abstract Recent advancements in foundation engineering have introduced composite piles, specifically the Confined Concrete-Filled Aluminum Tube (CCFAT) pile system, which can effectively support both vertical and lateral loads. However, the behavior of composite piles under combined loading conditions remains largely unexplored. This research investigates the performance of CCFAT pile groups installed in loose sand and subjected to combined loads. Experimental studies focused on 1×2 and 2×2 CCFAT configurations with varying slenderness ratios (L_m/d) of 10, 15, and 20. These experiments were used to validate Finite Element (FE) models. Numerical simulations were then conducted for new configurations, including 2×3 and 3×3 CCFAT piles, to gather additional performance data. Results indicated that the ultimate vertical capacity of the CCFAT pile groups increased with the L_m/d ratio. Under combined loading, the ultimate lateral capacity also improved with higher vertical loads for a given L_m/d ratio. The laboratory findings showed a near-linear relationship between both ultimate vertical and lateral capacities and the L_m/d ratio. Failure mechanisms identified through numerical simulations revealed that CCFAT pile groups experienced punching shear failure, indicative of confined deep flow behavior. Under specific vertical loads, lateral loading resulted in soil compression on the right and tension on the left, causing heave and depression zones, significant soil yielding, and wedge formations. Sensitivity analyses highlighted that, for pure lateral loads, the internal friction angle and Young's modulus significantly affect CCFAT pile group behavior, while under vertical loads at 80% of ultimate vertical load (P_{uv}), the internal friction and dilatancy angles have a greater impact on lateral capacity than other parameters. Based on these findings, new expressions were proposed to calculate the ultimate lateral load (P_{ulv}) for CCFAT pile groups under combined loading conditions, integrating the identified influencing factors.

Keywords Composite piles · Confined concrete-filled aluminum tube · Combined loading · Ultimate lateral load

F. Al-Darraji (✉)
Department of Civil Engineering, College of Engineering, University of Basrah, Basrah, Iraq
e-mail: f.k.aldarraji@2021.ljmu.ac.uk

F. Al-Darraji · M. Sadique · Z. Yu · A. Shubbar · T. Marolt Čebašek
School of Civil Engineering and Built Environment, Liverpool John Moores University, Liverpool L3 3AF, UK
e-mail: m.m.sadique@ljmu.ac.uk

Z. Yu
e-mail: z.yu@ljmu.ac.uk

A. Shubbar
e-mail: A.A.Shubbar@ljmu.ac.uk

T. Marolt Čebašek
e-mail: t.maroltcebasek@ljmu.ac.uk

Published online: 02 January 2025

List of Symbols

C_c	Coefficient of curvature
C_u	Coefficient of uniformity
d	Pile diameter
D_{10}	Sand Effective size
D_{30}	Effective size
D_{50}	Sand medium diameter
d_r	Relative density
E	Young's modulus of soil
e_{max}	Maximum void ratio
e_{min}	Minimum void ratio
f_c'	Compressive strength of concrete cubes
G and λ	Empirical factors
G_s	Specific gravity
K	Friction coefficient
L_m/d	Slenderness ratios
P′	Atmospheric pressure
P_a	Mean principal stress
PIL	Percent improved lateral load
Pl	Lateral load
P_{lv}	Lateral load in the presence of a vertical load
P_{ul}	Ultimate lateral load
P_{ulwv}	Ultimate lateral load in the presence of a vertical load
P_{uv}	Ultimate vertical load
Pv	Vertical load
S	Centre to-centre distance between piles
γ_{max}	Maximum dry unit weight
γ_{mim}	Minimum dry unit weight
μ	Poisson's ratio
φ	Internal friction angle
ψ	Dilation angle

1 Introduction

Recently, there has been a growing demand for composite piles in civil engineering applications, particularly in marine structures. This is due to the fact that conventional foundations can be negatively affected by the harsh environmental conditions in these areas. Composite piles, which are made from a combination of materials such as steel and concrete, have emerged as a reliable solution for these critical applications (Harianto et al. 2023; M. A. Hosseini and Rayhani 2022). Composite piles offer several advantages over traditional piles (Al-Darraji et al. 2024). One primary benefit is their enhanced structural performance, combining the strength of multiple materials like concrete and steel to achieve better load-bearing capacities. Additionally, composites exhibit excellent corrosion resistance, ensuring longevity and reducing maintenance needs. Furthermore, their lightweight nature simplifies transportation and installation processes, contributing to increased efficiency and cost-effectiveness in construction projects.

In such sites, compound loads are frequently applied. Recently, numerous studies have addressed the behaviour of composite piles, the majority have predominantly focused on axial or lateral load scenarios. Since 1987, the development of various composite pile types, such as fiber-reinforced polymer (FRP) piles, steel core plastic (SCP) piles, Structurally Reinforced Plastic (SRP) piles, Plastic Lumber (PL) piles, and Fiberglass Pultruded (FP) piles, have been documented (Al-Darraji et al. 2023). Despite potential complications associated with pile driving and high damping attributed to composite pile materials, they present a viable alternative, particularly in corrosive environments (Shao et al. 2024). Globally, composite piles are increasingly incorporated into diverse projects owing to their adaptability and resilience (Almallah et al. 2020). These composite pile variants have found application in numerous infrastructure projects globally, including the Port of Los Angeles in 1987 (Horeczko 1995; Pando 2003), Hudson River Park in 1998 in New York (Zyka and Mohajerani 2016), The Shard in London, UK, in 2009 (Liu et al. 2022), and Marina Bay Sands in 2010 in Singapore (Coult et al. 2022). Recent studies have demonstrated that composite piles exhibit superior load-carrying capacity compared to conventional concrete piles (Fam et al. 2003; Mirmiran et al. 2002; Pando 2003). The promising capabilities of composite piles warrant further investigation into their performance under varying load conditions.

Despite the limited number of studies, prior research on composite piles has primarily focused on load transfer and their flexural response under axial or lateral loading (Mohammad Amin Hosseini and Rayhani 2017; Iskander et al. 2001; Manjunath et al. 2020). In a study conducted by Helmi et al.(2006), the impact of pile driving forces and high-cycle fatigue on the flexural performance of concrete-filled glass/carbon fiber-reinforced polymer (CFRP) piles was investigated. The results of the study showed that the driving forces had a relatively insignificant effect on

the flexural strength of CFRP piles, which displayed greater deflections compared to pre-stressed concrete piles. However, the FRP tubes required higher driving energy and demonstrated lower flexural resistance, which increased the likelihood of buckling. In a recent experimental study performed by Lu et al. (2022) on the behaviour of fibre-reinforced polymer piles in sandy soils, various factors influencing the performance of FRP piles under vertical and lateral loads in sandy soil were investigated. The study utilized a specialized pressure chamber for testing purposes. The findings highlighted that soil shearing resistance and the bearing capacity of FRP piles under vertical loads were primarily influenced by factors such as surface roughness, confining pressure, and relative density. Furthermore, the flexural stiffness of the piles was found to be influenced by the type of FRP, pile size, and climate age, indicating a significant impact of these variables on the structural behavior of the piles. Giraldo and Rayhani (2014) examined hollow FRP piles under vertical and lateral static loads, revealing a higher axial load-carrying capacity compared to similar steel pipe piles. However, the flexural rigidity of FRP piles was found to be less than that of steel counterparts, suggesting potential weaknesses in compound loading scenarios. Hollow steel piles and steel piles filled with concrete were investigated under axial and lateral loading conditions, considering various length-to-diameter ratios (10, 15, 20, 25, and 30) to emulate the behavior of stiff piles. Experimental results were validated through comparison with FE simulations. Collective findings from both experimental assessments and numerical analyses indicated that increasing length-to-diameter ratios resulted in enhanced load-carrying capacity and reduced settlement for both types of piles (Venkatesan et al. 2022).

The behavior of a pile group subjected to both vertical and lateral loads is more complex than the behavior of a single pile under only lateral or vertical loads, as observed by Choi et al. (2017) and Hazzar et al.(2017). The interaction between piles and the additional resistance provided by the cap in a pile group leads to a more complicated overall response, resulting in increased stress on the piles and the formation of distinct load patterns on the structure. However, the conventional approach in pile design primarily uses single-pile capacity estimation to predict the lateral capacity of pile groups, which can be attributed to the limitations and lack of a clear theoretical foundation for handling combined loading in traditional pile design. This results in confusion regarding the impact of vertical loads on the lateral response of piles and a scarcity of literature on the combination of vertical and lateral loads. The limited information available on this aspect, derived from analytical investigations (Liang et al. 2015; L. M. Zhang et al. 2002) and laboratory studies (Klein and Karavaev 1979; Li et al. 2020), indicates that, for a given lateral load, the presence of a vertical load tends to diminish the lateral resistance. Conversely, some laboratory (Anagnostopoulos and Georgiadis 1993; Mu et al. 2018) and FE studies (Achmus and Thieken 2010; Conte et al. 2013; Ramadan et al. 2024) suggest an increase in lateral capacity when subjected to vertical loads. However, from numerical studies, Achmus and Thieken (2010) conducted a series of FE analyses to assess the pile response in non-cohesive soil under combined vertical and lateral loads using the commercial FE software ABAQUS. The results revealed that during the initial stages of vertical load application, the lateral stiffness of the soil increased considerably, leading to an elevation in the lateral capacity load of the pile. Beyond a threshold value, the escalating vertical load induced a significant increase in lateral soil deformation, accompanied by a sudden decrease in soil stiffness.

Methods based on continuum principles, such as FE modeling, provide a way to overcome the constraints associated with current techniques in use. Over the past decade, advancements in computational capabilities of contemporary computers have facilitated an increasing prevalence of comprehensive pile group modeling through the application of the FE method. Hussien et al. (2012) observed a marginal increase in the lateral bearing capacity of piles embedded in sandy soil under vertical load, as evidenced by simplified 2D FE analyses. Investigations by Prendergast and Gavin (2016) as well as Wu et al., (2018) delineated the deformation response of piles subjected to simultaneous vertical and lateral loadings, demonstrating an increase in lateral displacement with increasing vertical loads, where the application of Winkler springs was incorporated. Advanced constitutive models prove valuable in capturing the non-linear responses of both soil and piles, explicitly considering group effects, geometric considerations, non-linearities such as detachment and sliding at the soil–pile interface, and diverse load

conditions (Franza and Sheil 2021; Karthigeyan et al. 2006). Despite their computational costs, a major challenge of using these methodologies is the need to calibrate and validate advanced constitutive models, which requires extensive testing.

Research on composite piles, particularly under combined loading conditions, faces significant challenges due to the limited focus on their behavior compared to traditional piles, especially regarding simultaneous vertical and lateral loads. Conventional design methods often rely on single-pile capacity estimates, which overlook complex interactions in pile groups. Additionally, soil variability and the high damping characteristics of composite materials during driving complicate load-bearing assessments. This study aims to investigate the combined load performance of Confined Concrete-Filled Aluminum Tube (CCFAT) piles in loose sand through experimental tests and Finite Element simulations. The purpose of the study is to enhance understanding of composite piles under complex loads, improve FE modeling to capture non-linear behaviors, and establish a theoretical foundation for the effects of vertical loads on lateral resistance. To achieve the objectives of this research, the following steps have been taken and presented in Fig. 1.

Phase one The experimental setups were designed to apply vertical, lateral, and combined loads (vertical and lateral) on fabricated scaled pile group system, having known material properties.

Phase two A series of experimental model tests were executed within a soil chamber, elucidating the behavior of 1×2 and 2×2 CCFAT pile groups. The investigation encompassed varying slenderness ratios (L_m/d) ratios of 10, 15, and 20 in loose sand, all under the influence of combined loading conditions involving both vertical and lateral loads. Given that piles are typically not structurally designed to resist lateral loads; particular emphasis is placed on the influence of the vertical load on the lateral response of CCFAT pile groups-an aspect of paramount importance for design engineering. The study explored the response of 1×2 and 2×2 CCFAT pile groups under combined load conditions.

Phase three: In this phase, beyond providing insights into evolving resistance mechanisms and their interactions, the experimental results serve as a benchmark for validating the corresponding FE models. The FE simulations were performed in ABAQUS.

Phase four: Following successful validation at the model scale, the investigation extends to evaluate new configurations, specifically 2×3 and 3×3 arrangements for CCFAT pile groups, forming a parametric study. Subsequent to this analysis, the study explores the variation of lateral soil stress variation around CCFAT piles under varying combined load conditions. Moreover, in order to enhance the comprehensiveness of the research, a sensitivity analysis is conducted, accounting for variations in soil properties and the coefficient of friction between CCFAT piles and the surrounding soil.

Phase five: In the final phase, the knowledge developed and gained through the experimental investigation and FE analyses were summarised to improve the existing knowledge and understanding of composite pile groups under combined loading. As well as the finding design codes that consider realistic structural and environmental loading were proposed.

2 Experimental Test

2.1 Experimental Setup

The experimental setup comprises a soil chamber, a square-sectioned enclosure crafted at Liverpool John Moores University (LJMU), with dimensions of 900×900 mm in plan and a height of 1250 mm. Configured for the application of combined loading (vertical and lateral), the experimental rig utilizes two hydraulic arms to apply concurrent vertical and lateral loads to the cap of a group of piles under the same testing regime. The target vertical load is centrally applied to the pile group caps through a sliding roller connection, crucial for facilitating free horizontal movement during lateral load application. The vertical load is quantified using a calibrated load cell attached to the sliding roller, connected to an adjustable pin with perforations along an extendable rod spanning up to 1500 mm. This rod is securely fastened to a vertical hydraulic arm, with the first hydraulic pump responsible for administering the vertical load. Maintaining a constant vertical load, the lateral load is incrementally applied in approximately 50 N increments until the final lateral load capacity is reached. The ultimate lateral capacity in this study is defined as the load corresponding to the lateral displacement equivalent to 10% of the pile diameter.

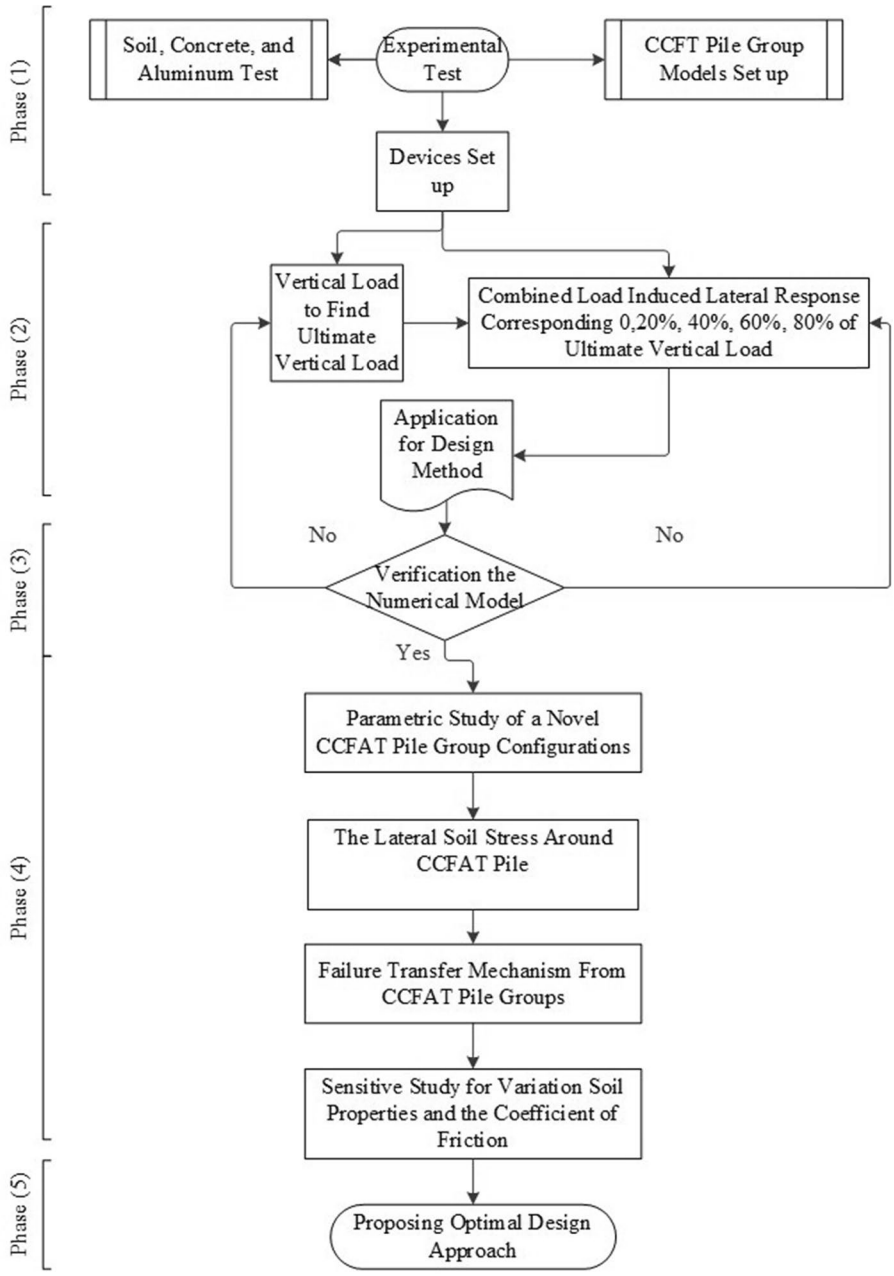

Fig. 1 The methodology of the research

This systematic procedure is applied to all pile group models to evaluate their response under combined loading.

Notably, combined load tests are conducted for vertical loads corresponding to the ultimate vertical load (P_{uv}) as follows: $0P_{uv}$, $20\%P_{uv}$, $40\%P_{uv}$, $60\%P_{uv}$, and $80\%P_{uv}$. The P_{uv} is conventionally defined as the load corresponding to the vertical settlement of 10% of the outer pile diameter (British Standards Institute 2020). In the lateral load system, the load cell, accompanied by the adjustable pile, is connected to a horizontally oriented hydraulic arm directed toward the pile model head. The other end of the horizontal hydraulic arm is linked to the second hydraulic pump, responsible for generating the lateral load. To mitigate rotational effects induced by lateral load on the pile model cap, a steel plate measuring (200×10 mm) is interposed between the load cell and the pile model

cap. Concurrently, two horizontal LVDTs monitor lateral displacements, while a 16-bit resolution data acquisition system records vertical and lateral loads, as well as lateral displacements. Figure 2a, b and c present the section, front, and top views of the testing rig respectively, illustrating the combined loading systems.

2.2 Soil Properties and Preparation of Test Chamber

In the experimental setup, a homogeneous, fine-grained sand with a quartz content of 96.5% was used within the soil chamber. The morphology and dimensions of sand particles represent pivotal factors influencing the shear behavior of granular materials, as articulated by Dyskin et al. (2001). Göktepe and Sezer (2010) affirmed that alterations in sphericity, roundness, or angularity correlate with variations in the minimum void ratio (e_{min}) and maximum void ratio (e_{max}) of the sand. This investigation utilized Scanning Electron Microscopy (SEM) at 57 × magnification and a Working Distance (WD) of 14.7 mm to analyze the morphology of sand particles, revealing sub-rounded characteristics that contribute to a higher unit weight in comparison to rounded particles as can be shown in Fig. 3a. According to the Unified Soil Classification System criteria, the sand can be categorised as poorly graded (SP). The sand, categorized as loose with a Relative Density (d_r) of 30%, adheres to the physical properties outlined in Table 1. The shear strength property, specifically the internal friction angle (φ), was experimentally determined through direct shear tests following the BSI (1994). Adhering to the scaling law standards, a ratio of 112 between the pile diameter and the sand medium diameter (d/D_{50}) was maintained, as depicted in Fig. 3b. This conforms to the recommended ratio of 60 Jebur et al. (2021).

To prepare the loose sand bed, the pouring and tamping technique, as prescribed by Basack (2009), Khari et al., (2013), Reddy and Ayothiraman (2015), and Al-abboodi and Sabbagh (2018) and Aamer et al. (2024) was used. This involved the systematic division of the chamber height into 50 mm layers. Sand, pre-quantified and weighed, was then meticulously transferred to the testing chamber using a scoop. To attain the desired relative density, the scoop was gradually lowered into the soil chamber until it reached the level of the previously poured sand layer. Subsequently, a hand compactor was utilized to compact the sand to the appropriate depth for each layer. The cumulative density required was achieved by systematically tamping these layers of sand.

2.3 CCFAT Pile Group Models

The CCFAT pile model constitutes a composite arrangement of piles. The aluminum tubes used are having an external diameter of 38.1 mm and a wall thickness of 1.6 mm. The formulation of the concrete mix for filling the aluminum tube in the composite pile model is predicated on the knowledge of the compressive strength of concrete cubes (f_c'). An optimal water-cement ratio (w/c) is ascertained through this process. The concrete composition in this investigation comprises Type I Portland cement, gravel, natural sand, water, and a superplasticizer. The coarse and fine aggregates exhibit gradations of 1–6 mm and 0–3 mm, respectively. Cubes measuring 100 mm on each side have been produced for ongoing strength monitoring**.** As depicted in Fig. 4a, all components are thoroughly blended, stirred, and subsequently poured into the aluminum tubes. The design parameters for the concrete mix are briefly outlined in Table 2.

The lengths of CCFAT piles are deliberately selected to depict slenderness ratios (L_m/d) of 10, 15, and 20, as specified by Pujiastuti et al. (2022). For the experimental combined loading test, two configurations have been devised to represent the pile group models of CCFAT 1 × 2 and CCFAT 2 × 2 configurations. As illustrated in Fig. 4b, instances of CCFAT pile group models were subjected to combined loading. Pile caps with diverse dimensions were fabricated using aluminum plates with a thickness of 20 mm. The configuration of holes drilled through the cap aligns with the specified arrangement of pile. The center to-center distances between piles in the group models adhere to three pile diameters (S = 3d), as detailed by Comodromos et al., (2009). The geometric and loading details considered in this study have been tabulated in Table 3.

3 Results

3.1 Experimental Investigation

3.1.1 Vertical Capacity of CCFAT Piles

The crucial importance of the lateral response of piles in engineering design is the main focus of this

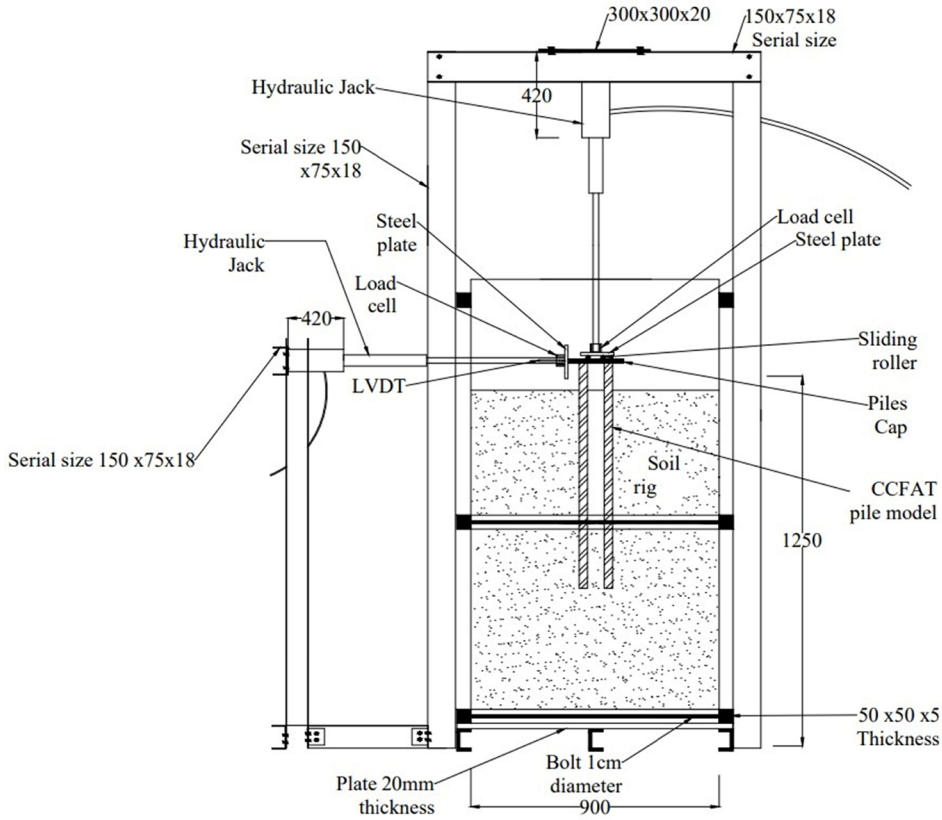

(a) Section view for testing CCFAT pile group 2x2 configuration (dimensions in mm)

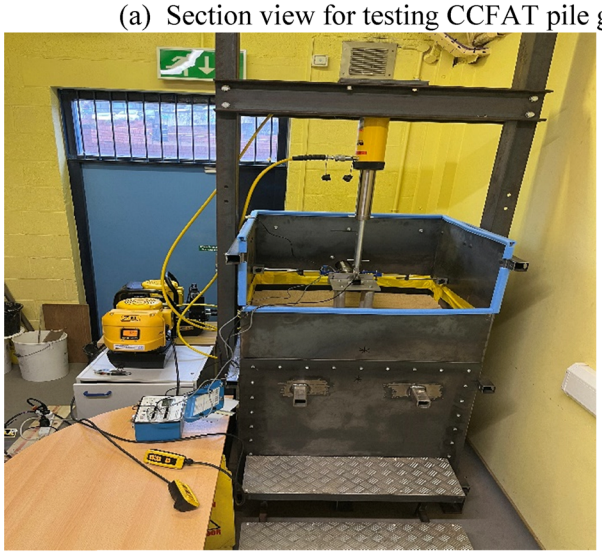

(b) Front view for testing CCFAT pile group 2x2 configuration

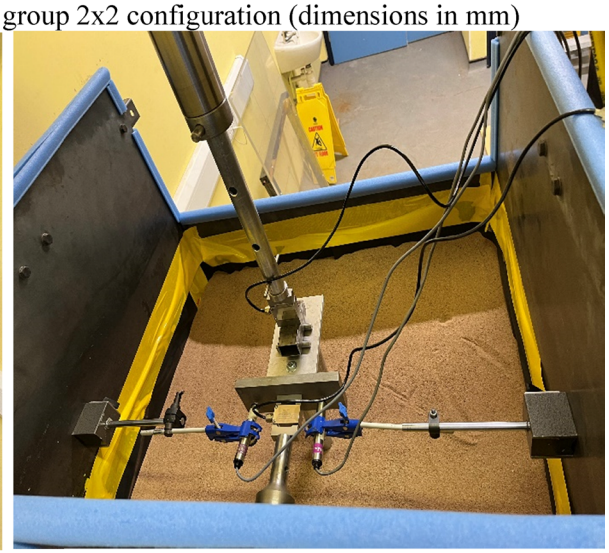

(c) Top view for testing CCFAT pile group 1x2 configuration

Fig. 2 The combined loading systems

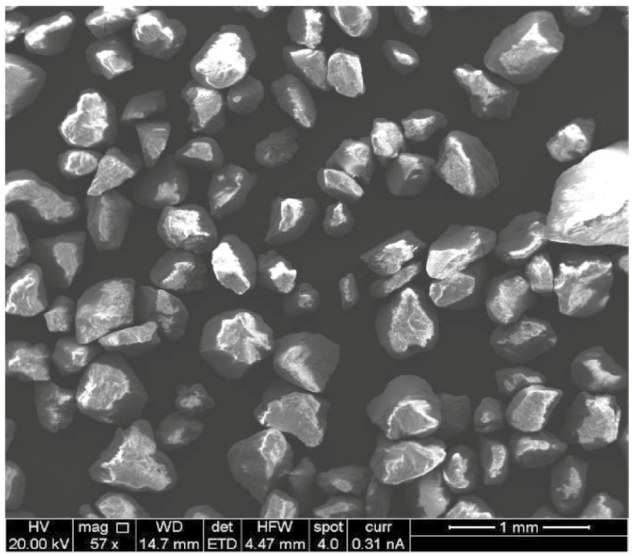

(a) Scanning electron microscopy (SEM) examination on sand particles, wherein HV and mag denote high voltage and magnification, while WD, det, ETD, and HFW represent working distance, detector, Everhart-Thornley detector, and horizontal field width, respectively.

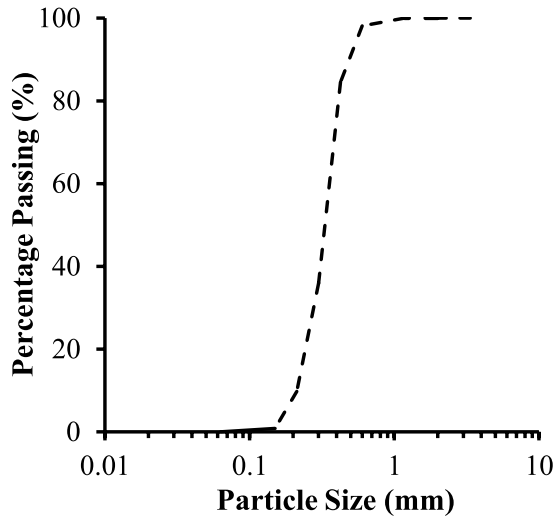

(b) Sand size-based distribution of particles

Fig. 3 Sand characterises

Table 1 Physical characteristics of the sandy soil employed in the experimental program

Soil characterise	Value
Coefficient of curvature (C_c)	1.11
Coefficient of uniformity (C_u)	1.9
Effective size, D_{10} (mm)	0.21
Effective size, D_{30} (mm)	0.29
Mean grain size, D_{50} (mm)	0.35
Particle size range (mm)	0.063–0.95
Maximum dry unit weight, γ_{max} (kN/m^3)	17.53
Minimum dry unit weight, γ_{mim} (kN/m^3)	15.51
Specific gravity, G_s	2.65
Maximum void ratio, e_{max}	0.71
Minimum void ratio, e_{min}	0.48

investigation. In this study, the concurrent load scenario is approached as a vertical-lateral load combination, with a specific focus on delineating the impact of the vertical load on the lateral response of CCFAT pile groups. Consequently, the vertical load is administered to the CCFAT pile model preceding the application of the lateral load. Initial scrutiny involves the independent evaluation of the ultimate vertical load (P_{uv}) for each CCFAT group model in the experimental test. Subsequently, in the second scenario, the vertical load is incrementally applied to a predetermined value, as discussed above. Following this, the lateral load is introduced at the cap of the pile model in increments of approximately 50 N until it attains the ultimate lateral load capacity, under the constant vertical load.

Figure 5a and b present the vertical load versus vertical settlement curves for CCFAT pile groups of 1×2 and 2×2 configurations, respectively. In this study, the ultimate vertical capacity (P_{uv}) has been defined as the vertical load that corresponds to a settlement of 10% of pile diameter. For a pile diameter of 38.1 mm, from Fig. 5a, the ultimate vertical capacities of 1×2 CCFAT pile group corresponding to 3.81 mm settlement are obtained as 781.92, 892.17 and 1109.44 N for L_m/d ratios of 10, 15 and 20, respectively. Similarly, from Fig. 5b, the ultimate

(a) Casting CCFAT pile specimens

(b) CCFAT pile group models (2x2 and 1x2 configurations)

Fig. 4 Examples of CCFAT pile group models tested under combined loading

Table 2 Mixture properties of the experimental concrete

Parameters	Value
Cement-sand-aggregate ratio	1: 1.5: 2.5
Water-cement ratio	0.45
Super-plasticiser	1.5% to cement by weight
Compressive strength, f_c' (MPa)	30

Table 3 Geometric and loading details of experimental study

CCFAT Pile group geometry	Pile diameter (mm)	Slenderness ratio, L_m/d	P_{uv} (%)
1×2 pile group 2×2 pile group	40	10, 15, 20	0, 20, 40, 60 & 80

vertical capacity of 2×2 CCFAT pile group, the ultimate vertical capacities for L_m/d ratios of 10, 15 and 20 are obtained as 1611.60, 1919.25 and 2562.75 N, respectively.

The ultimate vertical capacity of CCFAT pile groups of 1×2 and 2×2 configurations have been noted to increase with L_m/d due to the contribution of both skin friction and end bearing resistance. The increased length leads to a greater surface area of the pile in contact with the soil, which results in increased skin friction resistance.

In order to investigate the variation of ultimate vertical capacity with L_m/d ratio, the vertical load capacity at failure for 1×2 and 2×2 are plotted with L_m/d ratios of 10, 15 and 20, respectively, shown in Fig. 6. From the figure, for 1×2 CCFAT pile group model, the ultimate vertical capacity is noted to increase in a near linear manner from 781.62 to 892.17 and 1109.44 N, respectively for L_m/d ratios of 10, 15 and 20 N. A similar variation is noted for 2×2 CCFAT pile group model. The ultimate vertical capacity for the 1×2 CCFAT pile group model is found to be 781.62 N for L_m/d value of 10. As the L_m/d ratio is increased to 15 and 20, the ultimate vertical capacity is noted to increase by 14.10% and 41.89%, considering L_m/d of 10 as a reference. For 2×2 CCFAT pile group model, the ultimate vertical capacity is found to be 1611.6 N for L_m/d of 10. As the L_m/d is further increased to 15 and 20, the ultimate vertical capacity is noted to increase by 19.09% and 59.02%, compared to L_m/d ratio of 10. For both 1×2 and 2×2 CCFAT pile group models, the ultimate vertical capacities are noted to increase in almost a linear manner.

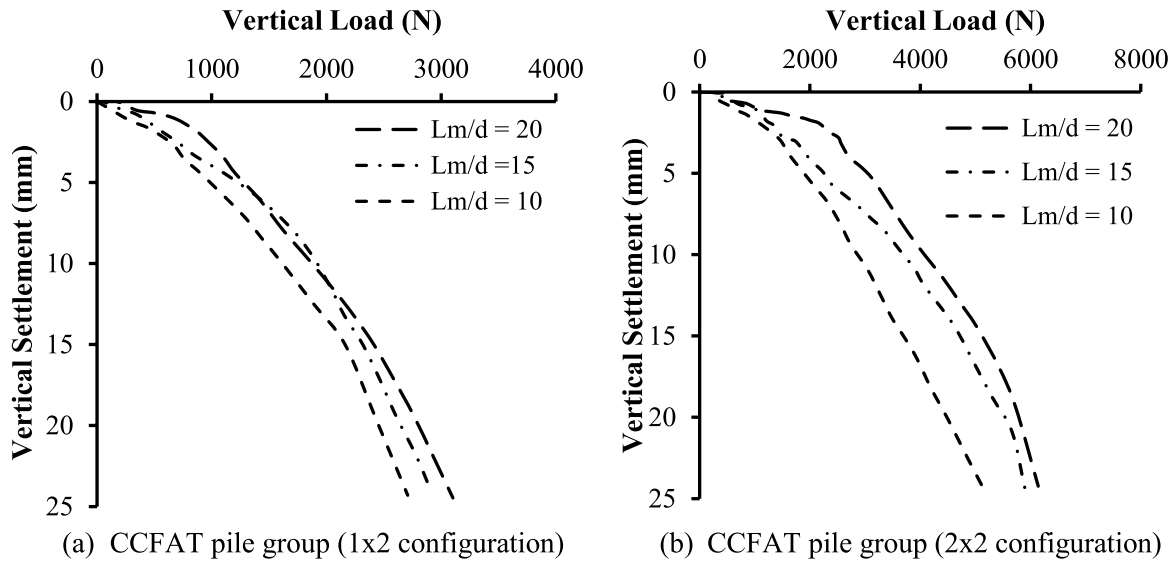

Fig. 5 Vertical load versus vertical settlement curves

3.1.2 Lateral Capacity of CCFAT Pile Group

Figures 7 and 8 show the variation of the combined load-induced lateral response of CCFAT pile group models 1×2 and 2×2, respectively, for L_m/d of 10, and 20. The experimental tests were conducted by varying the vertical loads from 0, 20, 40, 60, and 80% of the corresponding ultimate vertical load (P_{uv}) for CCFAT pile groups. From Fig. 7a, for L_m/d value of 10, the ultimate lateral capacity of 1×2 CCFAT pile group is noted to increase as the vertical load is increased from 0 to 80%. For example, the ultimate lateral load capacity is noted to increase from 336.50 to 359.90, 366.30, 382.10 and 382.10 N as the vertical load is increased from 0 to 20, 40, 60 and 80%, respectively. For the same CCFAT pile group configuration, the ultimate lateral capacities are noted to be higher for increased L_m/d values. For instance, for L_m/d ratio of 20, the ultimate lateral capacities are noted to increase from 487.50 to 499.50, 516.60, 524.80 and 526.99 N, respectively. Similar variation is noted for all the L_m/d ratios considered in this study for 2×2 CCFAT pile group, shown in Table 4.

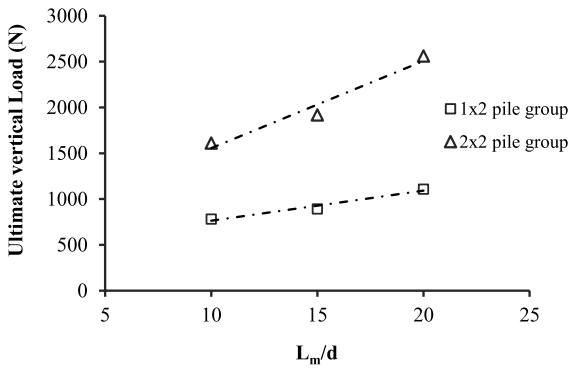

Fig. 6 Variation of ultimate vertical capacity with L_m/d

The lateral capacity increase with increasing vertical loads can be attributed to the densification effect caused by the vertical load (Deb and Singh 2023). This densification effect enhances the confining pressure around the CCFAT pile group, leading to an improvement in the lateral resistance. As vertical loads are applied to the CCFAT pile group, the surrounding soil experiences increased stress and compaction, which in turn enhances the lateral capacity. In addition, the increase in lateral capacity with increasing L_m/d ratios in sand is due to the increase in confining stress with depth. As the length of CCFAT pile group increases, the confining stress also increases, leading to an increase in the frictional resistance between the pile and the surrounding soil. This increase in frictional resistance results in a higher pile capacity (Deb and Singh 2023).

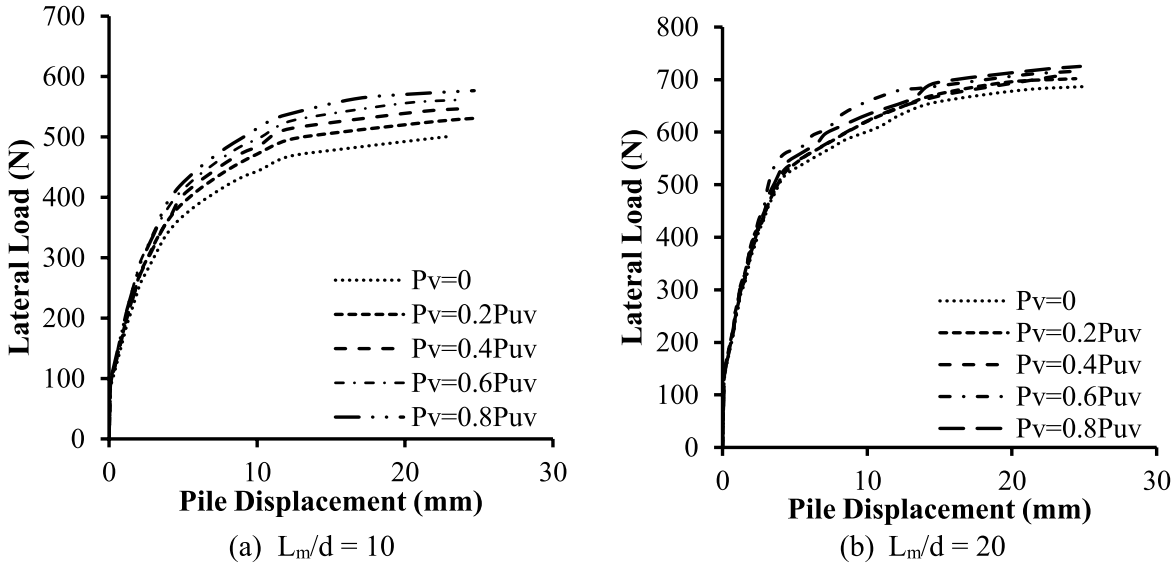

Fig. 7 Combined load-induced lateral response of CCFAT pile group model 1×2 configuration

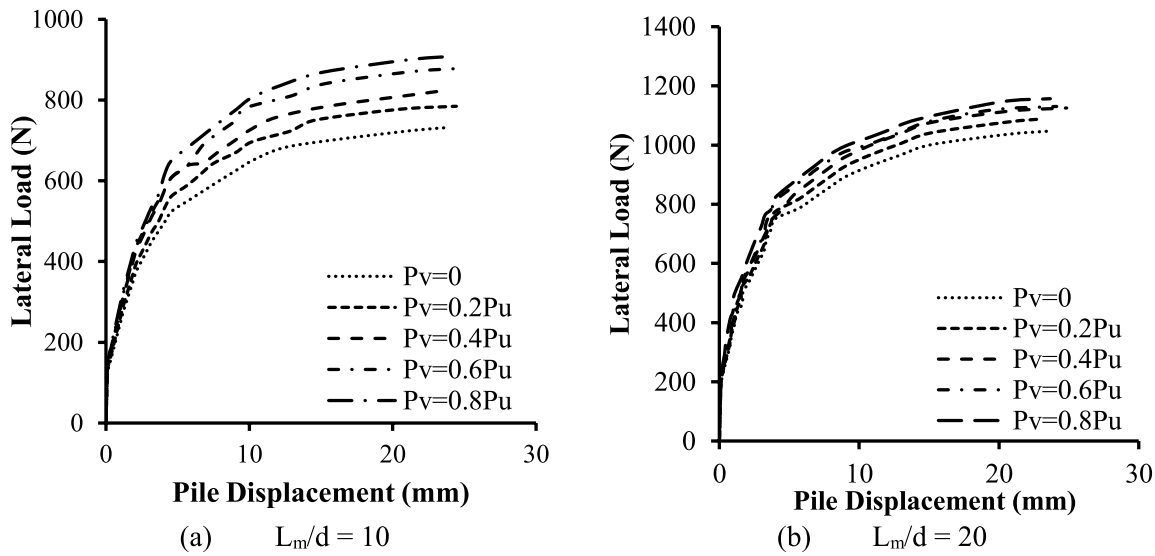

Fig. 8 Combined load-induced lateral response of CCFAT pile group model 2×2 configuration

3.1.3 Variation of Ultimate Lateral Capacity with Vertical Load and L_m/d

The variation of ultimate lateral load capacity with the vertical load applied in increments of 0, 20, 40, 60 and 80% of ultimate vertical capacity for 1×2 and 2×2 CCFAT pile groups are shown in Fig. 9. From the figure, for a given pile group and constant L_m/d ratio, the ultimate lateral capacity is noted to increase with increasing vertical load. For instance, for 2×2 CCFAT pile group having the L_m/d ratio of 20, the ultimate lateral capacity is noted to increase in a nearly linear manner from 743.80 to 764.80, 775.70,

Table 4 Ultimate lateral capacity of CCFAT pile groups

L_m/d	P_v (%)	Ultimate lateral capacity (N)	
		1×2 CCFAT pile group	2×2 CCFAT pile group
10	0	336.50	482.90
	20	359.90	509.70
	40	366.30	550.70
	60	382.10	561.50
	80	391.50	576.20
15	0	417.20	646.50
	20	427.05	671.80
	40	444.30	678.40
	60	456.30	702.30
	80	463.20	726.40
20	0	487.50	743.80
	20	499.50	764.80
	40	516.60	775.70
	60	524.80	791.80
	80	526.99	800.10

791.80, and 800.10 N as the vertical load is applied corresponding to 0, 20, 40, 60 and 80% of the ultimate vertical load. Also, for a given value of vertical load value, the ultimate lateral capacity is noted to increase with the L_m/d ratio. For example, for the 2×2 CCFAT pile group and vertical load corresponding to 20% of ultimate vertical load, the ultimate lateral load capacity is noted to increase from 509.70 to 671.80 and 764.80 N for L_m/d values of 10, 15, and 20, respectively. Similar variation is noted for all the geometries considered in this study.

The ultimate lateral capacities of 1×2 and 2×2 CCFAT pile groups obtained from Figs. 7 and 8 have been plotted against L_m/d for 0, 40 and 80% of ultimate vertical capacity and is shown in Fig. 10. From the figure, for any given pile group configuration and at constant L_m/d, the ultimate lateral capacity is noted to increase almost linearly with increasing vertical load. For example, in the case of 1×2 pile group and for a constant L_m/d ratio of 10, the ultimate lateral capacity is noted to increase to 336.50, 366.30 and 391.50 N for vertical load corresponding to 0, 40 and 80% of ultimate vertical load. Keeping all parameters constant, the 2×2 CCFAT pile group configuration always showed higher lateral capacity as compared to 1×2 CCFAT pile group configuration. Similar variation has been observed for all the geometries considered in this study.

In addition, from Fig. 9, for the 1×2 CCFAT pile group having a L_m/d value of 10, the ultimate lateral capacities were found to increase by 6.95, 8.86, 13.55 and 16.34% for the applied vertical load values of 20, 40, 60 and 80% of ultimate vertical capacity, respectively, considering pile group under pure lateral load as reference. For the same geometry, considering the pile group under pure lateral load as a reference, for an increased L_m/d value of 20, the ultimate lateral capacities were noted to increase by 2.46, 5.97, 7.65 and 8.10% for the applied vertical loads corresponding to 20, 40, 60 and 80% of ultimate vertical capacity, respectively. It can be noted that for a smaller L_m/d ratio, the influence of applied vertical load on ultimate lateral capacity is higher as compared to a higher L_m/d ratio. This trend finds support

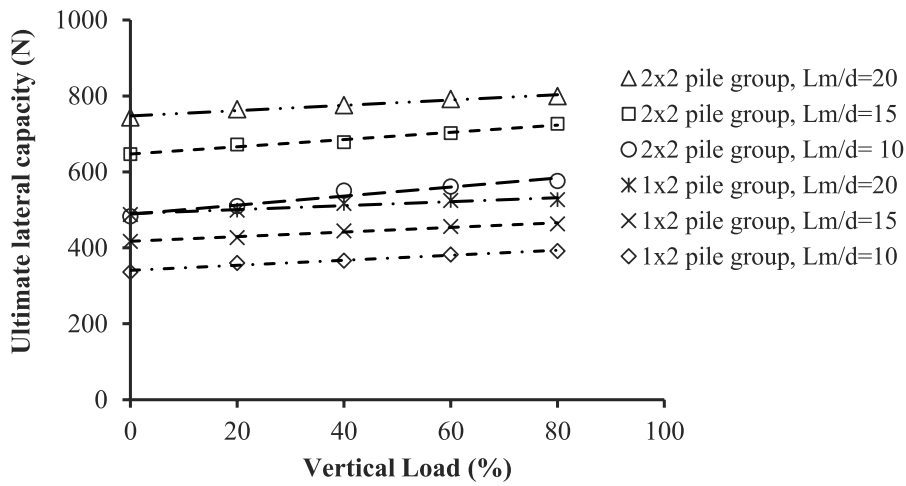

Fig. 9 Variation of ultimate lateral capacity with vertical load (%)

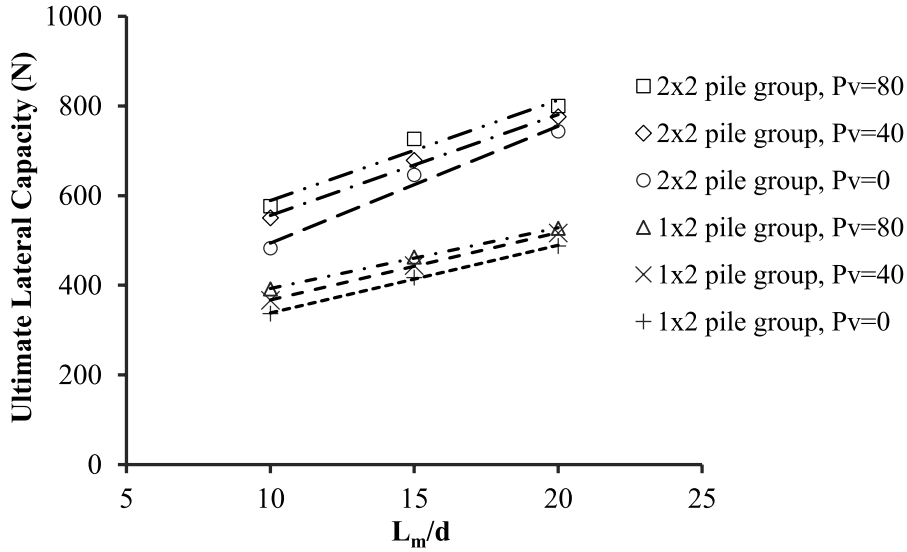

Fig. 10 Variation of ultimate lateral capacity with L_m/d

in the relatively higher percentage increase in lateral soil stress for short piles as opposed to their longer counterparts.

3.2 Numerical Analysis

To investigate the lateral response and load transfer mechanism at failure of CCFAT pile group foundations under combined loads, numerical simulations were carried out in ABAQUS.

The numerical simulation steps were first validated by comparing the results with experimental tests.

The CCFAT pile group foundation comprises aluminum and concrete components. Based on the conversion of engineering stress and strain for aluminum from coupling tests to true stress and logarithmic plastic strain, the aluminum tube and pile cap were modeled as linear elastic materials. For aluminium, Young's modulus of 70 GPa, Poisson's ratio of 0.3, and density of 27 kN/m^3 have been considered. To model the behaviour of concrete, Young's modulus of 25 GPa, a Poisson's ratio of 0.16, and a density (γ) of 24 kN/m^3, were considered. The behavior of the lose sand bed was simulated using the Mohr–Coulomb elastoplastic constitutive model with a non-associated flow rule. The soil non-linearity was captured by defining the modulus of elasticity as expressed in Eq. 1 (Deb and Singh 2018):

$$Es = P \times Pa\left(\frac{P'}{Pa}\right)^{\lambda} \quad (1)$$

Here, Pa represents the mean principal stress, $P\prime$ is atmospheric pressure, and G and λ are empirical factors. The soil properties, obtained from laboratory tests and calibrated with various numerical models (Amaludin et al. 2023; Bhowmik et al. 2016; Castilla-Barbosa et al. 2024; Z. Wang et al. 2023a, b), are detailed in Table 5.

The FE analyses were initially carried out to validate the vertical and lateral loads versus displacement results by comparing them with experimental results. For vertical load response, the geometries considered are 1×2 for L_m/d of 10 and 2×2 pile groups for L_m/d value of 20. For lateral load response, 1×2 of L_m/d value of 20 and 2×2 pile group with L_m/d value of 10

Table 5 Properties of sand

Soil parameters	Value
Young's modulus, E (MPa)	20
Empirical factor, G	600
Empirical factor,λ	0.55
Internal friction angle, φ (°)	30
Unit weight, γ (kN/m^3)	16.06
Dilation angle, ψ (°)	5
Poisson's ratio, μ	0.2

were considered under the applied vertical load corresponding to 0 and 80% of ultimate vertical loads.

Thereafter, the FE simulations were performed for pile groups of 2×3 and 3×3 configurations for L_m/d value of 15 under the applied vertical load corresponding to 0, 20, 40, 60 and 80% of ultimate vertical load.

The discretized FE models of soil domain, CCFAT pile group (2×2 configuration) and assembly mesh, are illustrated in Figs. 11a–c, respectively. Due to geometric and loading symmetry, only half of the CCFAT pile group embedded in the soil deposit was modelled. The lateral and vertical extents of soil domain were chosen large enough to avoid boundary effects. First-order, eight-node linear brick elements with reduced integration (C3D8R) were utilized to model soil domain and CCFAT pile group. To improve the accuracy of the solution, finer meshes were used in the vicinity of the pile group, the mesh size was gradually increased as the distance from the pile group increased in the horizontal direction. Boundary

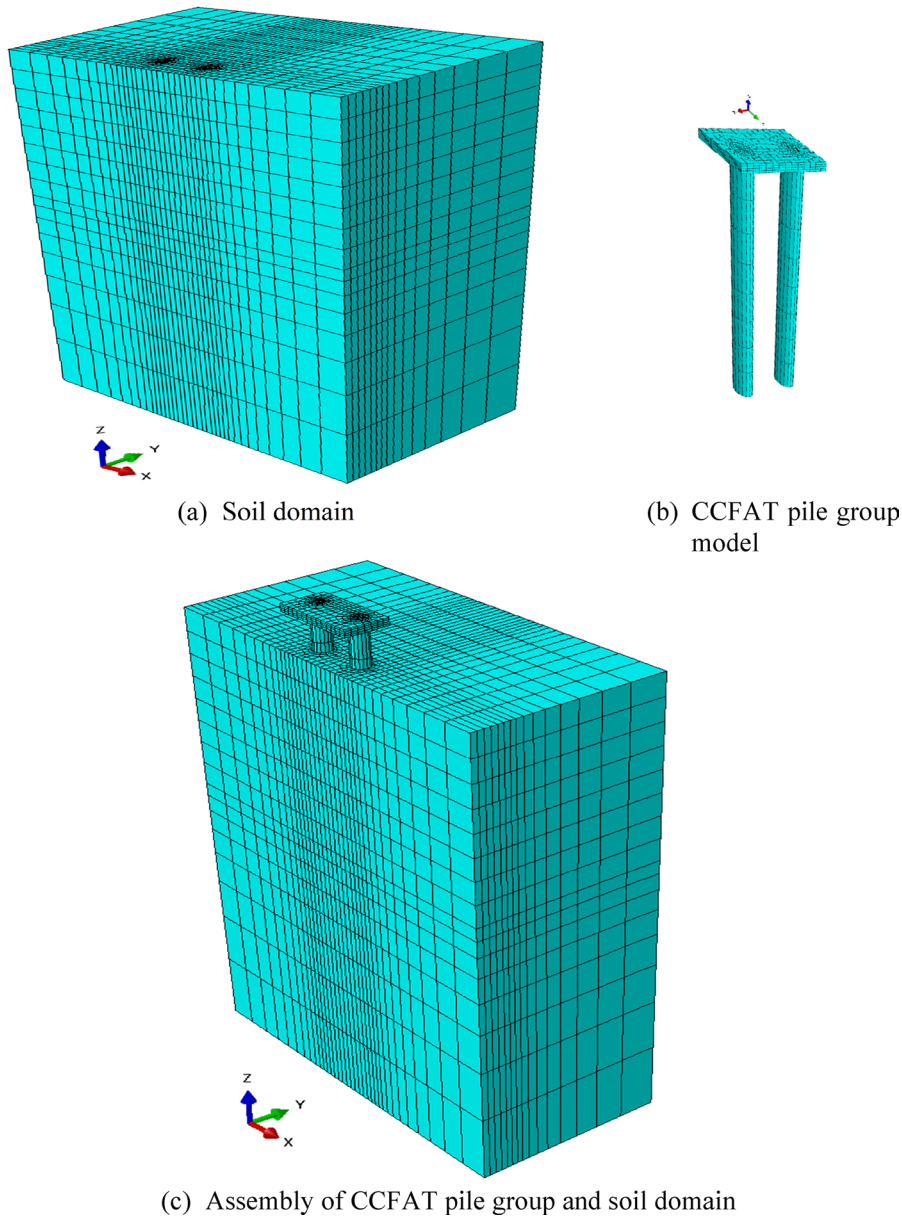

(a) Soil domain

(b) CCFAT pile group model

(c) Assembly of CCFAT pile group and soil domain

Fig. 11 Mesh description for CCFAT pile group of 2×2 configuration ($L_m/d = 10$)

conditions were implemented by restraining the bottom boundary of the soil deposit in all directions, while the vertical boundaries were constrained in the horizontal direction. The normal displacements were restricted within the symmetric plane.

To accurately capture interactions, a surface-to-surface contact approach was employed to establish contact between the soil and the external surface of the CCFAT pile model, as well as the contact between the inner surface of the aluminum tube and the outer surface of the concrete compound. Specifically, the contact was established by defining the outer surface of the aluminum tube as the master surface and the soil surface as the slave surface. Conversely, for the contact between the aluminum tube and the concrete compound, the outer surface of the concrete compound was designated as the master surface, while the inner surface of the aluminum tube acted as the slave surface. The interface governing these interactions was modeled using the "hard" contact model with Coulomb's tangent friction, and a specified friction coefficient between the CCFAT pile and soil was 0.3 (Fattah and Hamood 2023). No slippage was allowed between the aluminum tube and concrete surfaces. To replicate the combined load conditions from the experimental test, the loads were applied in sequential steps. In the first step, geostatic load was applied to establish the initial stress state across the entire soil domain. In the second step, contact between the external surface of the CCFAT pile model with soil and the inner surface of the aluminium tube with the outer surface of the concrete were established. In the third and final steps, the same sequence of load applications used in the experimental test was followed in the current FE analysis. In the third step, vertical load is applied at the top of the pile group. In the final step, the displacement controlled lateral load is applied at the top centre of the pile group till failure. In order to ensure a consistent and representative loading scenario, the sequence of vertical and lateral loads applied in the FE model was the same as that used in the laboratory experiments. In the numerical simulations, the installation effects were neglected, and the pile groups were assumed to be wished in place.

3.3 Numerical Study

3.3.1 Validation of FE Model

The accuracy and reliability of the present FE analysis were validated by comparing the predicted numerical model with experimental test models across three stages. The selected pile models comprised a 1×2 model with a L_m/d of 20 and a 2×2 model with a L_m/d ratio of 10, introducing variations in both pile configurations and L_m/d. In the initial stage focusing on vertical load, Fig. 12a shows the numerical predictions against the experimental test results in terms of vertical load in relation to the vertical settlement response of the chosen CCFAT pile group models. The close agreement between the numerical predictions and experimental results is evident for both group models. Additionally, a satisfactory alignment is observed between the numerical models and experimental tests concerning P_{uv}. Nevertheless, the disparity between the predicted and measured P_{uv} loads is less than 12% and 11% for the 1×2 and 2×2 models, respectively.

During the second and third stages, the outcomes of combined loading in the numerical model were juxtaposed with those obtained from experimental tests conducted under similar combined loading conditions. These stages involved the utilization of models featuring zero vertical loads and 80% P_{uv}. This was carried out to substantiate the iterative procedure employed in the proposed numerical models under conditions of limited and substantial vertical loads. Figure 12b illustrates a comparative analysis between numerical predictions and experimental results for combined loading, specifically for the CCFAT pile group 2×1, where zero and 80% of P_{uv} constituted the vertical loads. The numerical model accurately captures the curves spanning the entire spectrum of responses, from small-strain stiffness to the markedly non-linear regime. Regarding ultimate lateral load, the discrepancy between experimental and numerical models is confined to 14% and 12% for zero and 80% P_{uv} vertical loads, respectively.

In Fig. 12c, the lateral load–lateral displacement curves derived from the numerical models were depicted alongside the corresponding experimental data results for the CCFAT pile group 2×2, featuring a L_m/d of 10, under conditions of zero vertical load and 80% of P_{uv}. It is observed that, across both load

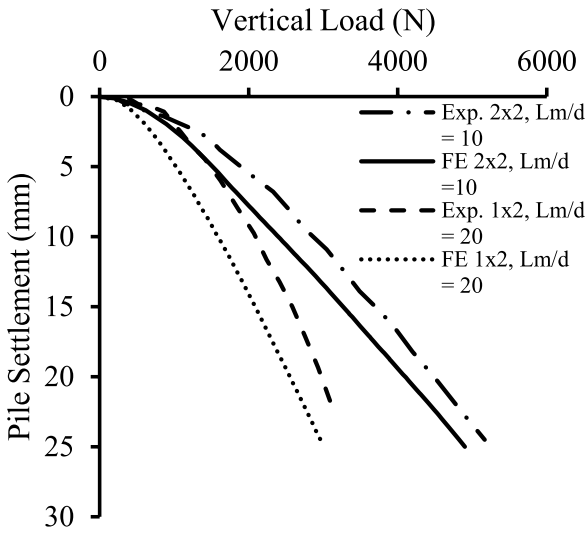

(a) CCFAT pile groups under vertical load

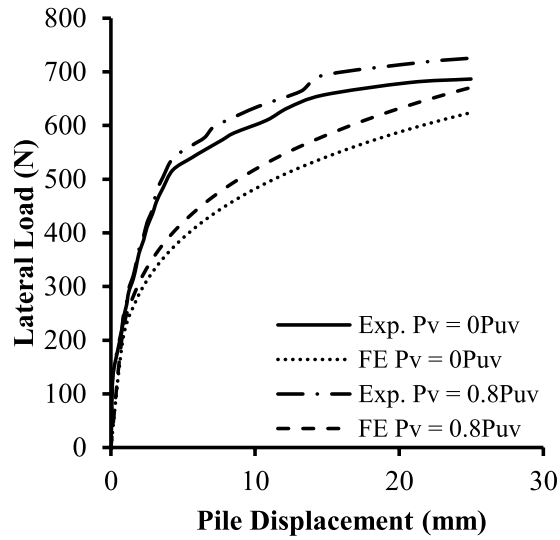

(b) CCFAT pile group 1x2, L_m/d =20 under combined load

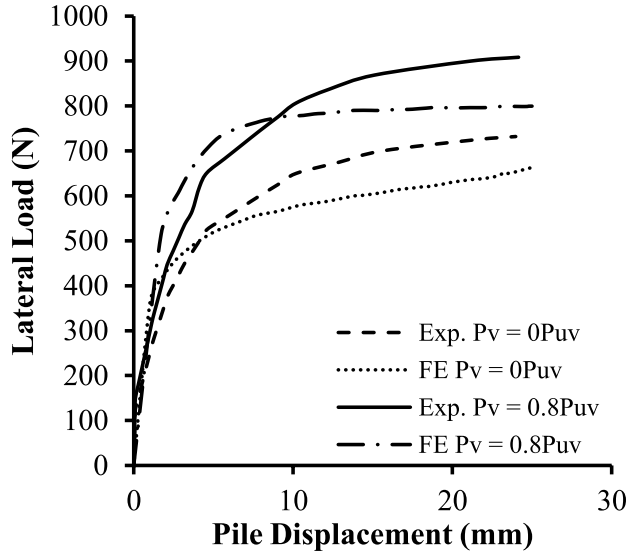

(c) CCFAT pile group 2x2, L_m/d =10 under combined load

Fig. 12 Verification the numerical models to experimental results

stages, the initial stiffness of the numerical models is marginally higher than that observed in the experimental tests, while the overall capacity tends to be reasonably conservative compared to the experimental outcomes. It is noteworthy that measuring the initial stiffness in small displacement zones poses significant challenges due to equipment limitations (Wang et al. 2022). Nevertheless, the comparative results suggest that the numerical models exhibit reasonable concordance with the experimental tests, demonstrating similar trends in the lateral load–lateral displacement curves. Furthermore, Fig. 12c effectively represents the predicted numerical results in terms of ultimate lateral load. The disparity between the experimental and numerical models remains below 3% and 6% for zero and 80% P_{uv} vertical loads, respectively.

In the various loading stages used to validate the numerical models, several common observations

can be summarized from Figs. 12a, b and c: (1.) The calculated numerical model curves exhibit smoother profiles compared to the experimental test curves. (2.) The stiffness of the numerical models is slightly lower than that observed in the experimental tests. This discrepancy in stiffness may be attributed to the simplifications employed in the simulation approach, particularly in representing the contact between the soil and both the outer surface of the CCFAT pile model and the inner aluminum surface of the concrete compound. Such simplifications are necessary to address the inherent complexities of real-world scenarios involving composite piles in soil.

Despite these differences, the numerical model successfully reproduces key aspects of the observed CCFAT pile group, accounting for variations in L_m/d under different loading conditions. This successful reproduction enhances confidence in using the numerical model for an investigational parametric study, which aims to generate additional performance data across diverse configurations of CCFAT pile groups under combined loads.

3.3.2 Parametric Study

Due to the constraints imposed by experimental test conditions, a parametric investigation was undertaken utilizing rigorously validated numerical models. Prior research efforts, as exemplified by Zhang et al. (2023), scarcely addressed the potential advantages inherent in the extensive array of possibilities within FE spaces and composite piles with group configurations. The present study focuses on a unique 2×3 and 3×3 configurations of CCFAT pile groups, maintaining a L_m/d ratio of 15, thereby establishing the novelty of both group piles and a distinct composite pile type.

Figure 13a and b illustrate the relationship between combined load-induced lateral load and lateral displacement for CCFAT pile group models 2×3 and 3×3, respectively. These figures comprehensively depict the outcomes of numerical tests conducted with varying vertical loads (0, 20, 40, 60, and 80% of P_{uv}) for CCFAT pile groups.

The ultimate lateral capacities of 2×3 pile group are found to be 827.71, 943.10, 974.50, 995.50 and 1047.90 N under the vertical load corresponding to 0, 20, 40, 60 and 80% of ultimate vertical capacities, respectively. Similarly, the ultimate lateral capacity of 3×3 pile group foundation is found to be 1168.60, 1366.40, 1442.30, 1472.70 and 1528.20 N, respectively for vertical load applied corresponding to 0, 20, 40, 60 and 80% of ultimate vertical capacities.

Observations from these figures reveal three consistent patterns in the responses of CCFAT pile group models 2×3 and 3×3 under the considered combined loading conditions: i) an increase in vertical load leads to a significant increase in lateral load at a

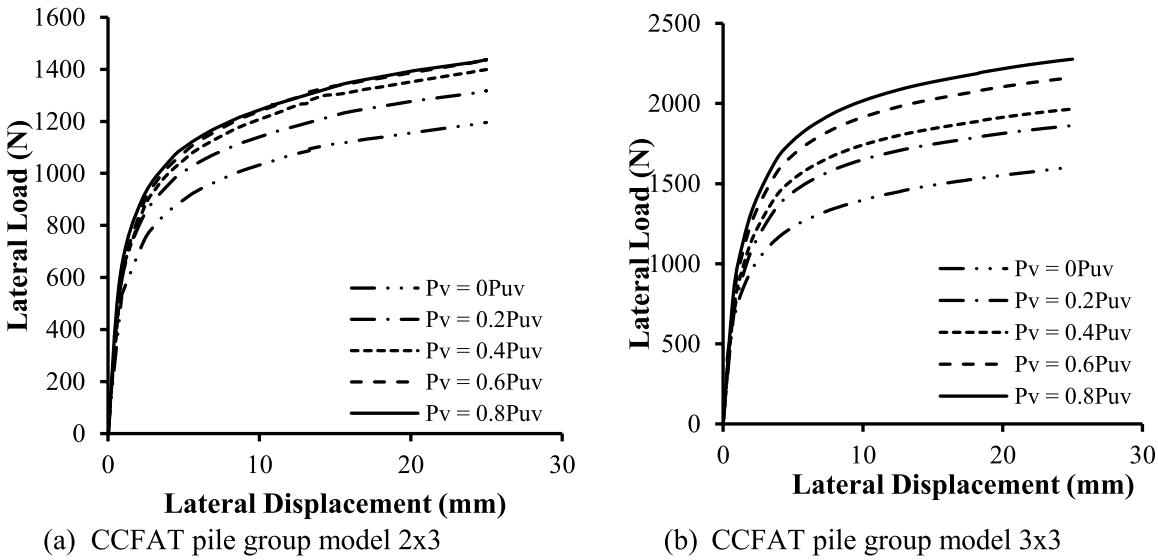

Fig. 13 Numerical results combined load-induced lateral response ($L_m/d = 15$)

given lateral displacement; ii) During the linear stage, a moderate increase in lateral capacity is evident, in contrast to more pronounced increases in the non-linear stages; iii) A uniform total lateral capacity is reached under all vertical loading conditions. These trends were elucidated further based on the experimental test results. These findings provide evidence suggesting that the distinctive behavior may arise from the stiffness of the composite pile, enhancing its resistance to lateral loads, particularly in the primary loading stages. Furthermore, the pile group exhibits the same failure type under lateral loads when subjected to vertical loading. However, it is noteworthy that the impact of vertical load on the lateral response of the CCFAT pile group was more pronounced in the 3×3 model compared to the 2×3 model.

3.3.3 The Lateral Soil Stress Around CCFAT Pile Group

Soil stresses pose formidable challenges that prove resistant to modification through experimental interventions (Peck 1969). Nevertheless, the expansive control capabilities inherent in numerical models offer a viable avenue to address this challenge, thereby enhancing the extensive database for improved engineering comprehension, particularly concerning the impact of combined loading on composite piles. Consequently, an in-depth exploration was undertaken to examine the lateral soil stresses resulting from both vertical and combined loads applied to groups of CCFAT piles. Further scrutiny was directed towards the evaluation of lateral soil stresses in front of CCFT pile group models 2×3 and 3×3, subjected to ultimate vertical load, pure ultimate lateral load, and ultimate lateral load, with an additional vertical load of $0.8P_{uv}$. The contour figures, denoted as 14, 15, and 16**,** depict the distribution of lateral soil stresses in the specified conditions. Irrespective of the sign, a positive value signifies lateral stress in the positive direction of the x-axis, while a negative value indicates stress in the opposite direction. Notably, the blue colour signifies the maximum stress value, whereas the red colour highlights the least affected zone.

From Figs. 14a and b, a comparative analysis of the contours illustrating lateral soil stress under ultimate vertical load (P_{uv}) is presented for CCFT pile group models 2×3 and 3×3. Notably, for both extremum models, the concentration of lateral soil stress is observed in close proximity to the base of the piles. This phenomenon can be attributed to the compression and downward movement of the soil, resulting in the densification of the soil under the influence of the vertical load. However, a discernible discrepancy

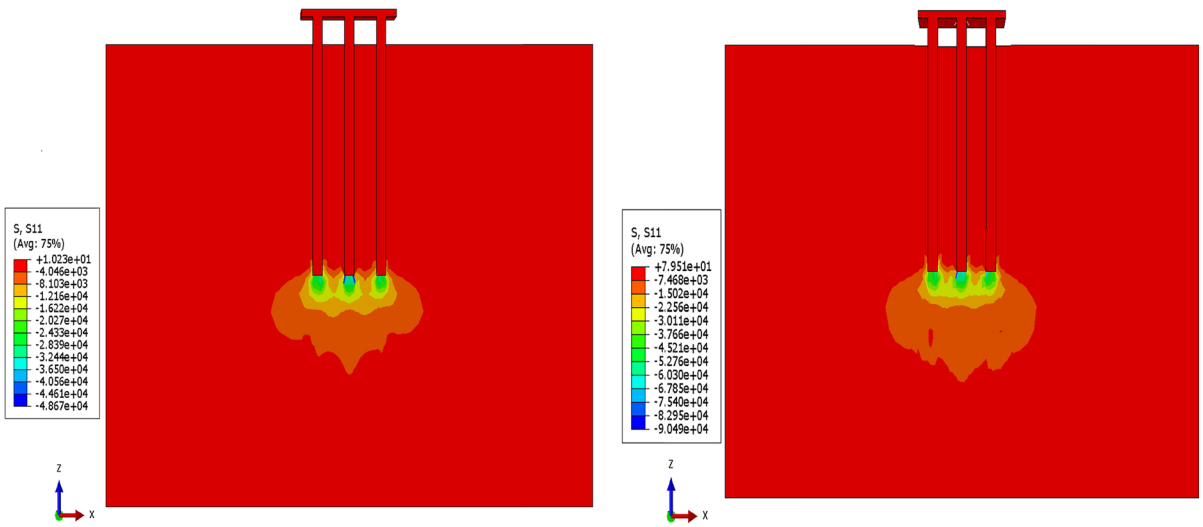

(a) CCFT pile group models (2x3 configuration)

(b) CCFT pile group models (3x3 configuration)

Fig. 14 Counters lateral soil stress for P_{uv}

is evident in the impact on the soil district between the CCFAT pile group 3×3 and 2×3 models. Specifically, the maximum lateral soil stress is markedly higher in model 3×3, reaching 9.049×10^4 N/m^2, compared to model 2×3, where it records 4.867×10^4 N/m^2. This increase in stress levels in the 3×3 model can be directly attributed to the higher ultimate vertical load experienced by the CCFAT pile group 3×3.

The lateral soil stress contours at pure ultimate lateral load for CCFAT pile groups models 2×3 and 3×3 at failure are shown in Figs. 15a and b, respectively. For the 2×3 pile group, in the rightmost pile of the pile group, the lateral stress is noted to increase from ground level in a parabolic manner along the pile depth, attains a maximum value at mid-depth of the pile and decreases at approximately 75% of the pile length. At the same load level, for the left most pile in the group, the lateral stress is noted to generate along the lower 25% (approximately) of the pile length. The variation remained similar for 3×3 pile group, with a higher magnitude of lateral stress. It is worth noting that the extent of the rightward lateral stress is significantly greater than that of the leftward lateral stress. This may attribute to the suggestion that the up-row pile falls within the active zone of the down-row pile, thereby experiencing a shadowing influence with the application of the lateral loads (Wen et al. 2020). On the other hand, the maximum lateral soil stress obtained from contour figures for analysis of the CCFAT pile group 3×3 models was slightly higher compared with 2×3 models. The maximum lateral soil stress for the CCFAT pile group 3×3 models was 6.648×10^3 and 5.638×10^3 N/m^2 for the 2×3 model.

Figures 16a and b illustrates the impact of the present vertical load at 80% of the P_{uv} through contours representing CCFAT pile groups 2×3 and 3×3, respectively. Analysis of the lateral soil stresses under these load conditions reveals an increase in both the lateral soil stresses and their influencing area around the ground and mid-level of down-row piles for both models. The observed increase in lateral soil stresses in these regions can be attributed to the compressive densification of the soil. Specifically, the vertical load is postulated to enhance the compression of the adjacent soil, consequently increasing soil stiffness. This phenomenon is denoted as the "soil densification effect." It can be inferred that the present vertical load magnifies the soil densification effect, providing additional insights into the reasons behind the amplified lateral load experienced by the CCFAT pile group when subjected to a vertical load (Nagai et al. 2024). Conversely, a conspicuous distinction is noted when determining the maximum lateral soil stresses between the two models. The maximum lateral soil stress in the 3×3 model is approximately twice that

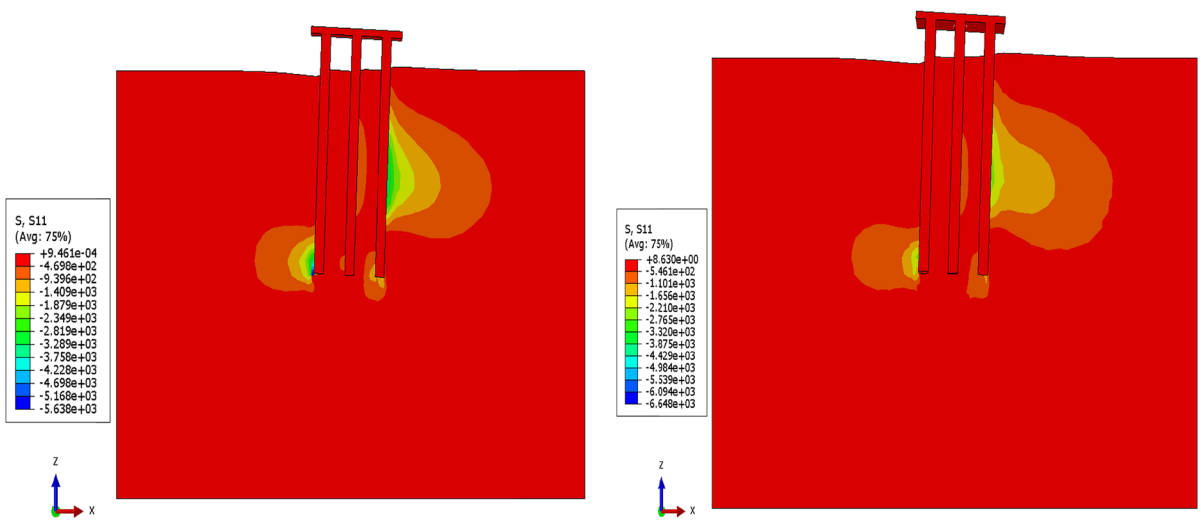

(a) CCFT pile group model (2x3 configuration) (b) CCFT pile group model (3x3 configuration)

Fig. 15 Counters lateral soil stress for Pure lateral load

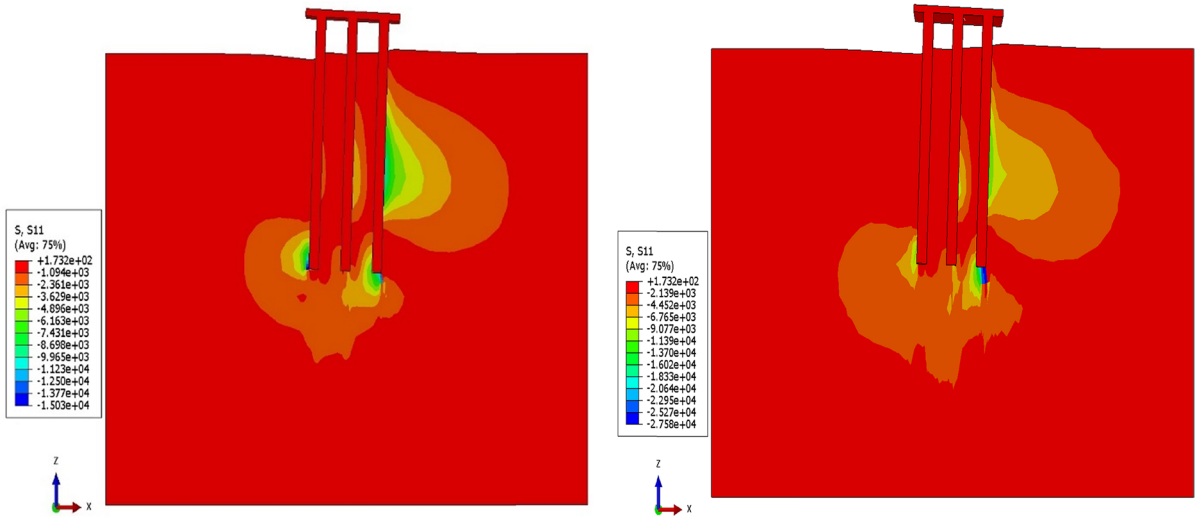

(a) CCFT pile group models 2x3 (b) CCFT pile group models 3x3

Fig. 16 Counters lateral soil stress with combined load ($P_v = 80\%P_{uv}$)

in the 2×3 model, a difference attributed to the larger ultimate vertical load value in the former. The maximum lateral stress is calculated at 1.503×10^4 and 2.758×10^4 N/m^2 for the CCFAT pile group models 3×3 and 2×3, respectively.

3.3.4 Failure Mechanism

Understanding the load transfer mechanism of CCFAT pile groups under vertical and combined loading is crucial for ensuring confidence in the design. The yielding of soil at the ultimate condition has been represented through plastic strain counter diagrams. Subsequently, an exhaustive investigation was conducted to scrutinize the plastic strain induced by vertical and combined loads applied to clusters of CCFAT piles. It is noteworthy that the colour red designates the maximum plastic strain, while the colour blue accentuates the least affected zone.

Figure 17a–b illustrate the generation of plastic strain diagrams under ultimate vertical loads for 2×3 and 3×3 CCFAT pile group models. In both models, the surrounding soil mass along the external interface of the piles is observed to undergo plastic yielding in the lower half of the embedment length. The plastic strain is noted to extend up to a certain depth below the tip of the piles. Both 2×3 and 3×3 CCFAT pile group models experience failure due to punching shear, and this is accompanied by the manifestation of a confined deep-flow mechanism. Under the vertical load, at failure, as compared to 2×3 pile group configuration, the magnitude of plastic stain was noted to be higher in the case of 3×3 pile group. Specifically, at the point of maximum plastic strain, there are conspicuously convergent values of 6.966×10^{-2} and 9.962×10^{-2} for CCFAT pile groups 2×3 and 3×3, respectively.

Figures 18 and 19 illustrate the failure mechanisms of 2×3 and 3×3 CCFAT pile groups subjected to lateral loads at failure, both under unloaded conditions and at 80% of the ultimate vertical loads. In response to these combined loads, the 2×3 and 3×3 CCFAT pile groups exhibited rotation around a central point, referred to as rotation centre, located at a specific depth beneath the ground. The upper half of the pile groups, as depicted in the figures, moved rigidly toward the direction of the applied lateral load, above the rotation center. Conversely, the lower half shifted leftward below the rotation centre, considering the mean position as a reference. Under the application of the lateral load, the tips of the leftmost piles in both groups shifted upward, while the tips of the rightmost piles penetrated deeper into the soil, relative to the mean position. At the ground surface level for both configurations, the soil on the right side of the pile groups experienced compression, causing

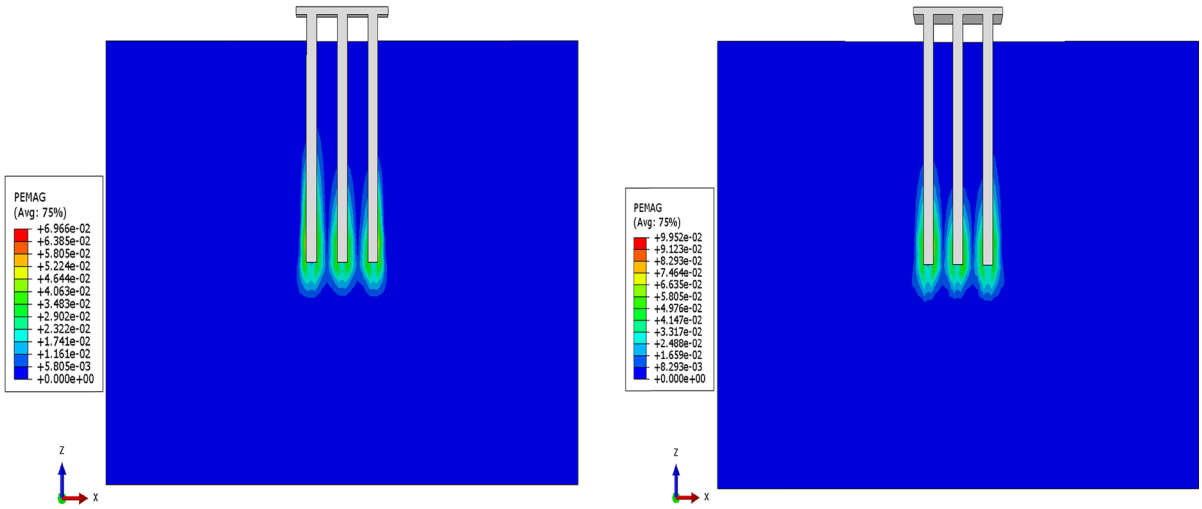

(a) CCFAT pile group models 2x3 (b) CCFAT pile group models 3x3

Fig. 17 Counters diagram of plastic strain for P_{uv}

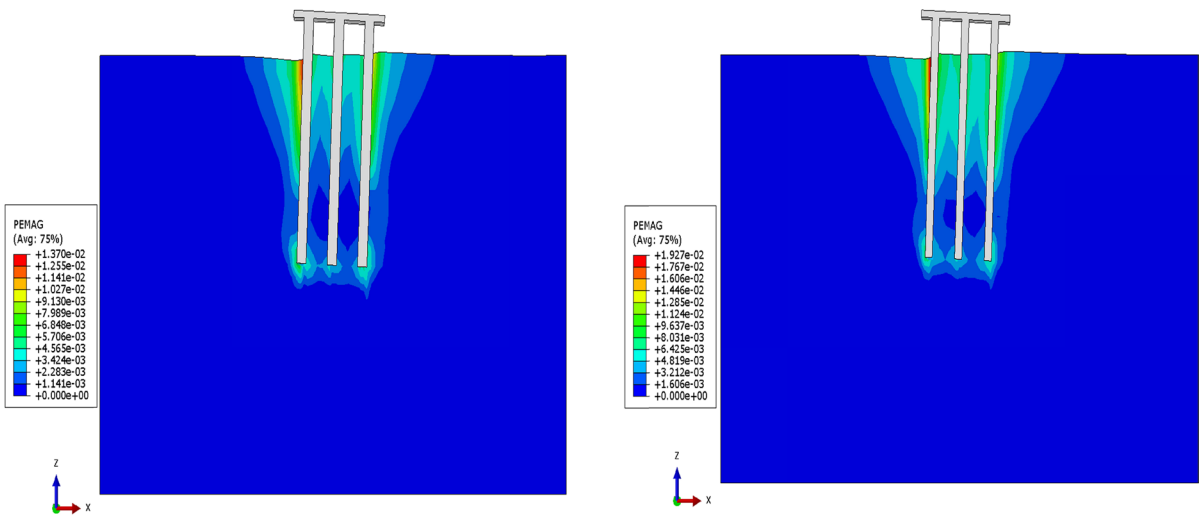

(a) CCFAT pile group models 2x3 (b) CCFAT pile group models 3x3

Fig. 18 Counters diagram of plastic strain for Pure lateral load

heave, while the soil on the left experienced tension, leading to the formation of a depression zone (Siacara et al. 2024). Due to the foundation displacement under combined loads, significant soil yielding in terms of plastic strains was noted in the soil mass between the piles within the group. Soil yielding appeared as wedge formations along the depth of the piles, most prominently on both the right and left sides at the surface level, with plastic deformation diminishing approximately 50–60% down the foundation depth. Notable deformations at the pile tips were also observed.

It is noteworthy from Figs. 18a and b that the maximum plastic strain, as deduced from contour

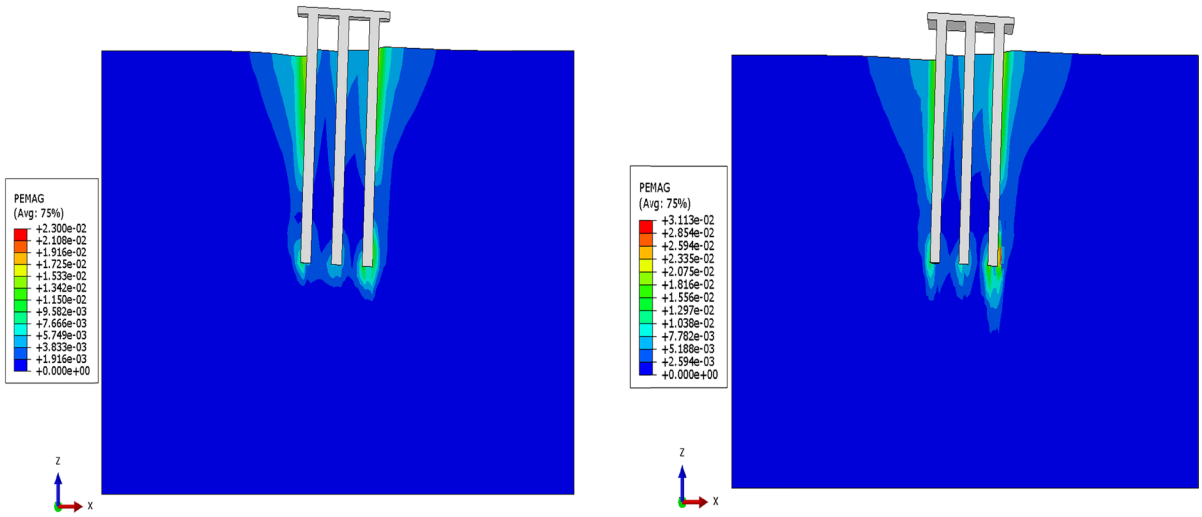

(a) CCFAT pile group models 2x3 (b) CCFAT pile group models 3x3

Fig. 19 Counters diagram of plastic strain for lateral load and vertical load ($P_v = 80\%P_{uv}$)

diagrams of CCFAT pile group 3×3 models, was higher when compared to 2×3 models. Specifically, the maximum plastic strain for the CCFAT pile group 3×3 models was 1.927×10^{-2}, while for the 2×3 model, it was 1.370×10^{-2}. Similarly, as illustrated in Figs. 19a and b, the maximum plastic strain values are 3.113×10^{-2} and 2.300×10^{-2} for the CCFAT pile groups of 2×3 and 3×3 configurations, respectively. The influence of applied vertical load for the pile groups at failure under lateral loads was studied by applying 0 and 80% of ultimate vertical loads for pile groups of 2×3 and 3×3 configurations. The plastic strain at failure is noted to increase with the applied vertical load. For example, from Figs. 18a and 19a, for 2×3 pile group, as the vertical load is increased from 0 to 80% of ultimate vertical, the plastic strain at failure is noted to increase from 1.37×10^{-2} to 2.30×10^{-2}. Similar variation is noted in the case of 3×3 pile group.

3.3.5 Sensitivity Analysis

Soil characteristics, encompassing factors such as internal friction angle, dilatancy angle, Young's modulus, and friction coefficient between CCFAT piles and soil, exert considerable influence over the densification of sand, constituting crucial elements in numerical modelling (X. Wang et al. 2023a, b; X. Zhang and Lu 2023). While certain factors, such as the internal friction angle, can be quantified through geotechnical assessments, challenges in measurement, particularly for the dilatancy angle, contribute to imprecise determinations. Consequently, a meticulous investigation was undertaken to evaluate the significance of these factors within the non-linear Mohr–Coulomb soil model. The soil parameters were varied within the practical range typically encountered in field applications to ensure relevance. The chosen parameters provide a basis for understanding the behavior of the CCFAT piles. The CCFAT pile group, configured as 3×3 with a L_m/d of 15, was designated as the control model. Table 6 presents the various parameters such as internal friction angle, dilatancy angle, Young's modulus, and friction coefficient between CCFAT piles and soil and their influence on lateral response under combined loading conditions. Each numerical

Table 6 Valuated soil factors

Parameters	Standard	Value
Internal friction angle, φ′ (°)	30	25, 35, 40
Dilatancy angle, ψ (°)	5	2, 10, 15
Young's Modulus, E (MPa)	20	10, 30, 40
Friction Coefficient, K	0.3	0.2, 0.4, 0.5

model underwent modification of a singular factor for detailed examination.

The impact of soil factors and the friction coefficient between CCFAT piles and soil is delineated in Figs. 20a and b, illustrating the response of the CCFAT pile group under both a pure lateral load scenario and a vertical load equivalent to 80% of P_{uv}, respectively. To elucidate the impact of the aforementioned factors more distinctly, the computed ultimate lateral loads were normalized against the initial loads for both loading conditions. In the case of pure lateral load, depicted in Fig. 20a, an increasing correlation demonstrated a substantial increase in the ultimate lateral load with increasing internal friction angle values within the range of 25°–40°, exhibiting a variation of 104%. The ultimate lateral load exhibited an increase with increasing dilatancy angle from 2°−15°, demonstrating a distinctive trend and resulting in a cumulative rise of 60%. With Young's modulus varying from 10 to 20 MPa, there was an increase in the ultimate lateral load by 36%. Conversely, when Young's modulus ranged from 30 to 40 MPa, the enhancement in ultimate vertical capacity was less than 19%. The impact of Young's modulus was more pronounced in loose sand conditions (10–20 MPa) compared to dense sand conditions (> 30 MPa). The friction coefficient between the pile and soil had a marginal effect, contributing to a 35% improvement within a reasonable range of friction coefficients (0.2–0.5). The internal friction angle and Young's modulus were identified as pivotal factors influencing the lateral behavior of the CCFAT pile group.

In the presence of vertical loads equivalent to 80% of P_{uv}, as depicted in Fig. 20b, the impact of the internal friction angle, ranging from 25° to 40°, demonstrated a substantial increase in ultimate lateral loads, by nearly 99%. Notable enhancements in ultimate lateral loads were observed, particularly in relation to variations in dilatancy angle from 2° to 15°. The behaviour exhibited a nearly linear relationship, manifesting a significant rise in ultimate lateral load with an increasing dilatancy angle, reaching a variation of 102%. Conversely, for diverse Young's modulus values spanning from 10 to 40 MPa, the ultimate lateral load exhibited approximately the same improvement trend as observed in the pure lateral load case, with an enhancement of 90%. Furthermore, this analysis illustrated that the influence of Young's modulus was less pronounced in dense sand conditions. Additionally, the ultimate lateral load was dependent on the friction coefficient between the pile and the soil. Nevertheless, the percentage improvement was comparatively lower than that associated with other considered soil factors, resulting in a 38% enhancement within

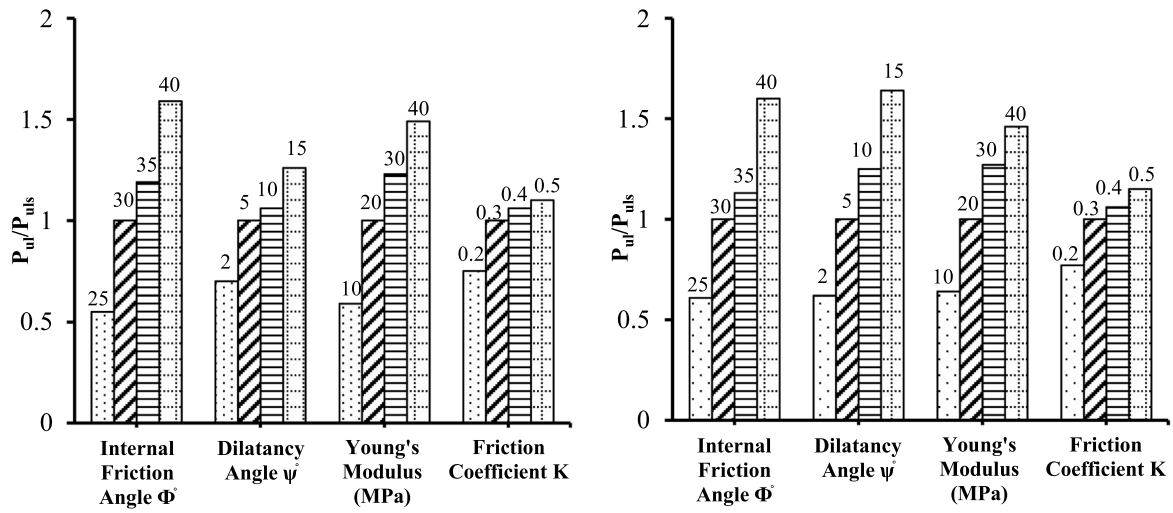

(a) Ultimate lateral loads, case of pure lateral load

(b) Ultimate lateral loads, presence of vertical load of 80% P_{uv}

Fig. 20 Influence combined loading with soil-sensitive factors on CCFAT piles group

a reasonable range of friction coefficients (0.2–0.5). In the presence of vertical loads equivalent to 80% of P_{uv}, internal friction angle and dilatancy angle were noted to have higher influence on the lateral load capacity as compared to the other parameters.

3.4 Design Expressions

The lateral capacities obtained at failure under various vertical loads and pure lateral capacities (under zero vertical loads) for 1×2, 2×2, 2×3 and 3×3 CCFAT pile groups were utilized to obtain Percent Improved Lateral load (PIL) (Karthigeyan et al. 2006). For a particular CCFAT pile group geometry, PIL can be obtained as the ratio of the difference between lateral capacity obtained at failure under various vertical loads and pure lateral capacity to pure lateral capacity (shown by Eq. (2)).

$$PIL = \frac{Plv - Pl}{Pl} \times 100\% \tag{2}$$

Here, P_{lv} represents the lateral load at a specific lateral displacement in the presence of a vertical load, and P_l denotes the lateral load at the same lateral displacement as P_{lv} under pure lateral load conditions. The variation of PIL for 1×2 and 2×2 CCFAT pile groups obtained from laboratory experiments is shown in Figs. 21a–c.

The lateral capacities obtained at failure under various vertical loads and pure lateral capacities (under zero vertical loads) for 1×2, 2×2, 2×3 and 3×3 CCFAT pile groups were utilized to obtain PIL. For a particular CCFAT pile group geometry, PIL can be obtained as the ratio of the difference of lateral capacity obtained at failure under various vertical loads and pure lateral capacity to pure lateral capacity (shown by Eq. (2)).

The laboratory investigation revealed that for a pile group size of 1×2 with a L_m/d of 10 (as shown in Fig. 21a, the increases in capacity percentages at vertical load levels of 20, 40, 60, and 80% of the ultimate vertical capacity were 6.97, 8.85, 13.55, and 16.34, respectively. Similarly, for a 2×2 pile group at the same L_m/d, the lateral capacity increased by 5.56, 14.04, 16.28, and 19.33% at these same vertical load levels of 20, 40, 60, and 80%, respectively. The data indicates that the PIL tends to rise almost linearly as the vertical load increases from 20 to 80% of the ultimate capacity. This trend of increasing PIL with higher vertical loads for all the pile groups and L_m/d ratios was consistent across all pile group configurations considered in the study.

Additionally, Fig. 21a illustrates specific observations for CCFAT pile group 1×2. From the figure, with L_m/d of 10, 20% increase in PIL has been observed when the vertical load corresponding to 80% of the ultimate vertical load was applied, compared to pure lateral loading condition. At the same vertical load level in Figs. 21b and c, with L_m/d at 15 and 20, PIL was observed to be 13% and 8%, respectively. From these figures, it can be observed that the increasing vertical load has an increasing effect on the ultimate lateral capacity. However, with increasing pile depth, it is evident that the PIL decreases considerably. Notably, when analysing PIL against the vertical load percentage for CCFAT pile group models, for example, 1×2 and 2×2 configurations, with the same L_m/d, a similar slope in the linear trend was observed. This suggests that the number of piles in the configurations 1×2 and 2×2 had a diminished effect on the PIL. This phenomenon may be attributed to the higher magnitude of ultimate vertical load for CCFAT pile group 2×2 compared to 1×2, encountering increased lateral resistance. Consequently, there was an approximately equivalent improvement in lateral load for the same percentage of present vertical load in both CCFAT pile groups 1×2 and 2×2. The variation remained similar for all the geometries considered in this study.

The data points obtained for each geometry plotted for PIL versus P_v/P_{uv} are utilized to arrive at the general form of relationship and can be expressed using Eq. (3). Here, *a* represents the slope or the coefficient of the linear relationship, and *b* is the y-intercept, indicating the value of PIL when the vertical load percentage is zero. The details of the coefficients for all the geometries have been presented in Table 7.

$$PIL = a \times \frac{Pv}{Puv} + b \tag{3}$$

Additionally, using Eqs. (2) and (3), the ultimate lateral load capacity in the presence of a vertical load (P_{ulv}) and can be expressed in terms of applied vertical load (in %), and pure lateral load using the general form given by Eq. (4). The details of the coefficients for all the geometries have been presented in Table 8.

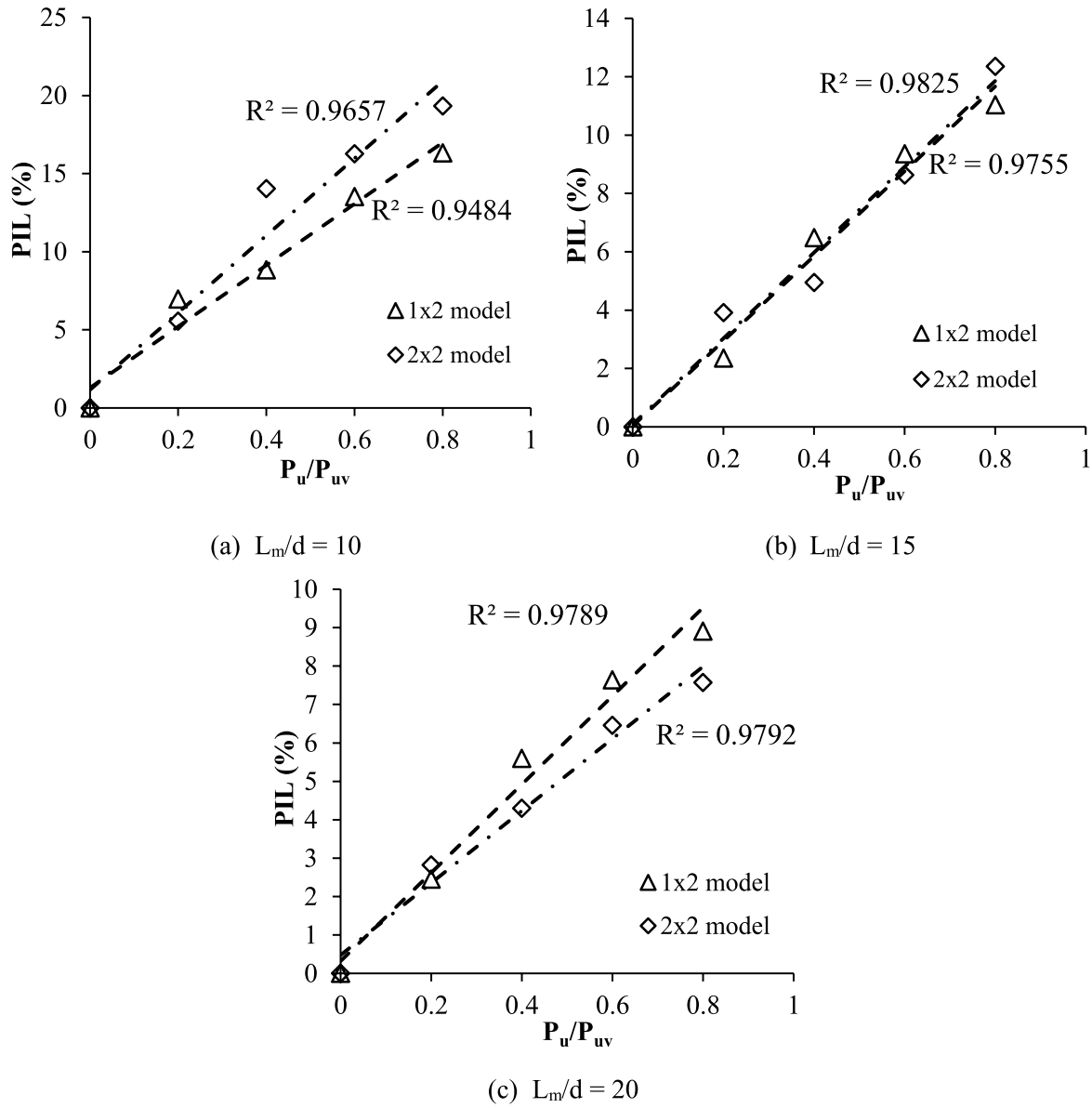

Fig. 21 Percent improved lateral load (PIL) vs the vertical load percentage

$$Pulv = \left(a\prime \times \frac{Pv}{Puv} + b\prime\right) \times Pul \times 10^{-2} \quad (4)$$

For a known value of *Pul* and $\frac{Pv}{Puv}$, the above expression can be utilized to predict the ultimate lateral load capacity within the range of parameters utilized in this study. The above expressions can serve as a preliminary guideline for the design of CCFAT pile group foundations.

4 Conclusion

Based on the laboratory experiments and finite element simulations performed on CCFAT subjected to combined vertical and lateral loading conditions are:

1. Vertical load greatly affects the lateral response of CCFAT pile groups, with capacity increasing as vertical load increases. The stiffness of

Table 7 Coefficients for determining PIL of pile group

Configuration	Coefficient	$L_m/d=10$	$L_m/d=15$	$L_m/d=20$
1×2 model	*a*	19.684	14.544	10.684
	b	1.290	0.031	0.555
2×2 model	*a*	24.691	14.711	9.388
	b	1.166	0.085	0.4758
2×3 model	*a*	–	0.291	–
	b	–	0.014	–
3×3 model	*a*	–	0.396	–
	b	–	0.041	–

Table 8 Coefficients for determining *Pulv* of pile group

Configuration	Coefficient	$L_m/d=10$	$L_m/d=15$	$L_m/d=20$
1×2 model	*a′*	19.684	14.544	10.684
	b′	101.290	100.031	100.555
2×2 model	*a′*	24.691	14.711	9.388
	b′	101.166	100.085	100.4758
2×3 model	*a′*	–	0.291	–
	b′	–	100.014	–
3×3 model	*a′*	–	0.396	–
	b′	–	100.041	–

the foundation improves lateral resistance, especially in early loading phases, resulting in capacity increase during nonlinear stages compared to linear stages.

2. The lateral behavior of piles subjected to combined loading is dependent upon the L_m/d ratio of the CCFAT pile. The impact of vertical load on the lateral response diminishes as the pile length increases. The CCFAT pile group 3×3, which has a higher ultimate vertical load, displayed significantly larger PIL values compared to the CCFAT pile group 2×3 model in FE simulations.
3. Vertical load significantly increases lateral soil stresses in CCFAT pile groups (2×3 and 3×3), particularly around the ground and mid-level of the down-row piles. During failure, the response of these pile groups under pure lateral and combined loads involves plastic yielding, causing notable soil deformation between the piles and forming plastic wedges along the pile depth. The greatest deformation occurs at the surface, decreasing to about 50–60% of the foundation depth.
4. Under pure lateral load conditions, the internal friction angle and Young's modulus were identified as crucial parameters. Furthermore, in the presence of vertical loads equivalent to 80% of P_{uv}, the dilatancy angle and internal friction angle had a significant influence on ultimate capacity.
5. Design expression was proposed to estimate the P_{ulv} for CCFAT pile groups which takes into account the pure lateral and vertical loads into account.

Funding The author(s) received no financial support.

Data availability Enquiries about data availability should be directed to the authors.

Declarations

Conflict of interest Authors declare that there is no conflict of interest.

References

Aamer F, Azzam W, Farouk A, Nasr A, Nazir A (2024) Uplift response of opening anchor bladed pile in sand. Geotech Geol Eng 42(7):6561–6583. https://doi.org/10.1007/s10706-024-02880-8

Achmus M, Thieken K (2010) On the behavior of piles in non-cohesive soil under combined horizontal and vertical loading. Acta Geotech 5(3):199–210. https://doi.org/10.1007/s11440-010-0124-1

Al-abboodi I, Sabbagh TT (2018) Model tests on piled raft subjected to lateral soil movement. Int J Geotech Eng 12(4):357–367

Al-Darraji F, Sadique M, Čebašek TM, Ganguli A, Yu Z, Hashim K (2023) A systematic review of the geotechnical and structural behaviors of fiber-reinforced polymer composite piles. Geosciences 13(3):78

Al-Darraji F, Sadique M, Alahmari TS, Zelong Y, Shubbar A, Cebasek TM (2024) Investigation of new confined concrete-filled aluminum tube piles: experimental and numerical approaches. Res Eng 24:103124. https://doi.org/10.1016/j.rineng.2024.103124

Almallah A, El Naggar H, Sadeghian P (2020) Axial behavior of innovative sand-coated GFRP piles in cohesionless soil. Int J Geomech 20(10):04020179. https://doi.org/10.1061/(asce)gm.1943-5622.0001808

Amaludin AE, Asrah H, Mohamad HM, Bin Amaludin HZ, Bin Amaludin NA (2023) Physicochemical and microstructural characterization of Klias Peat, Lumadan POFA, and GGBFS for geopolymer based soil stabilization. HighTech Innov J 4(2):327–348

Anagnostopoulos C, Georgiadis M (1993) Interaction of axial and lateral pile responses. J Geotech Eng 119(4):793–798

Basack S (2009) A technical note on development and performance study of a set-up for imparting lateral cyclic load on piles. Mar Georesour Geotechnol 27(4):322–341. https://doi.org/10.1080/10641190903143272

Bhowmik D, Baidya DK, Dasgupta SP (2016) A numerical and experimental study of hollow steel pile in layered soil subjected to vertical dynamic loading. Soil Dyn Earthq Eng 85:161–165. https://doi.org/10.1016/j.soildyn.2016.03.017

Choi YS, Lee J, Prezzi M, Salgado R (2017) Response of pile groups driven in sand subjected to combined loads. Geotech Geol Eng 35(4):1587–1604. https://doi.org/10.1007/s10706-017-0194-z

Comodromos EM, Papadopoulou MC, Rentzeperis IK (2009) Pile foundation analysis and design using experimental data and 3-D numerical analysis. Comput Geotech 36(5):819–836. https://doi.org/10.1016/j.compgeo.2009.01.011

Conte E, Troncone A, Vena M (2013) Nonlinear three-dimensional analysis of reinforced concrete piles subjected to horizontal loading. Comput Geotech 49:123–133. https://doi.org/10.1016/j.compgeo.2012.10.013

Coult G, Cannas A, Gregson S, Santelli L (2022) Apple marina bay sands: utmost transparency. Glass Struct Eng 7(3):363–380

Deb TK, Singh B (2018) Response and capacity of monopod caisson foundation under eccentric lateral loads. Mar Georesour Geotechnol 36(4):452–464

Deb TK, Singh B (2023) Bearing behavior of a monopod bucket foundation supporting an offshore wind turbine in sandy soils. Int J Geomech 23(10):04023180. https://doi.org/10.1061/IJGNAI.GMENG-8217

Dyskin AV, Estrin Y, Kanel-Belov AJ, Pasternak E (2001) Toughening by fragmentation—How topology helps. Adv Eng Mater 3(11):885. https://doi.org/10.1002/1527-2648(200111)3:11%3c885::AID-ADEM885%3e3.0.CO;2-P

Fam A, Pando M, Filz G, Rizkalla S (2003) Precast piles for route 40 bridge in Virginia using concrete filled FRP tubes. PCI J 48(3):32–45

Fattah MY, Hamood MJ (2023) Investigation on existing tunnel response to piles construction: a numerical study. Civil Eng J 9:202–216

Franza A, Sheil B (2021) Pile groups under vertical and inclined eccentric loads: Elastoplastic modelling for performance based design. Comput Geotech 135:104092. https://doi.org/10.1016/j.compgeo.2021.104092

Giraldo J, Rayhani MT (2014) Load transfer of hollow fiber-reinforced polymer (FRP) piles in soft clay. Transp Geotech 1(2):63–73. https://doi.org/10.1016/j.trgeo.2014.03.002

Göktepe AB, Sezer A (2010) Effect of particle shape on density and permeability of sands. Proc Inst Civ Eng Geotech Eng 163(6):307–320. https://doi.org/10.1680/geng.2010.163.6.307

Harianto T, Muhiddin AB, Arsyad A (2023) Soil reinforcement model test using timber pile at liquefaction area. Civil Eng J 9(6):1509–1521

Hazzar L, Hussien MN, Karray M (2017) On the behaviour of pile groups under combined lateral and vertical loading. Ocean Eng 131:174–185. https://doi.org/10.1016/j.oceaneng.2017.01.006

Helmi K, Fam A, Mufti A, Hall JM (2006) Effects of driving forces and bending fatigue on structural performance of a novel concrete-filled fibre-reinforced-polymer tube flexural pile. Can J Civ Eng 33(6):683–691

Hosseini MA, Rayhani M (2017) Evolution of pile shaft capacity over time in marine soils. Int J Geo-Eng 8:1–15

Hosseini MA, Rayhani MT (2022) Seismic evaluation of frictional FRP piles in saturated sands using shaking table tests. Soil Dyn Earthq Eng 163:1–12. https://doi.org/10.1016/j.soildyn.2022.107545

Hussien MN, Tobita T, Iai S, Rollins KM (2012) Vertical loads effect on the lateral pile group resistance in sand. Geomech Geoeng: Int J 7(4):263–282. https://doi.org/10.1080/17486025.2011.598571

Iskander MG, Hanna S, Stachula A (2001) Driveability of FRP composite piling. J Geotech Geoenviron Eng 127(2):169–176. https://doi.org/10.1061/(ASCE)1090-0241(2001)127:2(169)

Jebur AA, Atherton W, Al Khaddar RM, Loffill E (2021) Artificial neural network (ANN) approach for modelling of pile settlement of open-ended steel piles subjected to compression load. Eur J Environ Civ Eng 25(3):429–451

Karthigeyan S, Ramakrishna V, Rajagopal K (2006) Influence of vertical load on the lateral response of piles in sand. Comput Geotech 33(2):121–131. https://doi.org/10.1016/j.compgeo.2005.12.002

Khari M, Kassim KA, Adnan A (2013) An experimental study on pile spacing effects under lateral loading in sand. Sci World 2013:734292–734298. https://doi.org/10.1155/2013/734292

Klein GK, Karavaev VN (1979) Design of reinforced-concrete piles for vertical and horizontal loading. Soil Mech Found Eng 16(6):321–324. https://doi.org/10.1007/BF01710323

Li Q, Prendergast LJ, Askarinejad A, Gavin K (2020) Influence of vertical loading on behavior of laterally loaded foundation piles: a review. J Mar Sci Eng 8(12):1029. https://doi.org/10.3390/jmse8121029

Liang F, Zhang H, Wang J (2015) Variational solution for the effect of vertical load on the lateral response of offshore piles. Ocean Eng 99:23–33. https://doi.org/10.1016/j.oceaneng.2015.03.004

Liu Y, Feng T, Shi Z, He M (2022) Understanding the route choice behaviour of metro-bikeshare users. Transp Res Part a: Policy Pract 166:460–475

Lu Y, Abuel-Naga H, Shaia HA, Shang Z (2022) Preliminary study on the behaviour of fibre-reinforced polymer piles in sandy soils. Buildings 12(8):1–17

Madhusudan Reddy K, Ayothiraman R (2015) Experimental studies on behavior of single pile under combined uplift and lateral loading. J Geotech Geoenviron Eng 141(7):04015030

Manjunath RN, Khatkar V, Behera BK (2020) Investigation on seawater ageing of PET-epoxy composites: an ecological and sustainable approach for marine applications. J Polym Environ 28(8):2289–2300. https://doi.org/10.1007/s10924-020-01771-2

Mirmiran A, Shao Y, Shahawy M (2002) Analysis and field tests on the performance of composite tubes under pile driving impact. Compos Struct 55(2):127–135

Mu L, Kang X, Feng K, Huang M, Cao J (2018) Influence of vertical loads on lateral behaviour of monopiles in sand. Eur J Environ Civ Eng 22(sup1):s286–s301. https://doi.org/10.1080/19648189.2017.1359112

Nagai H, Takai T, Yasuda Y (2024) Simplified calculation of horizontal dynamic impedance of piled raft foundation on layered soil. Geotech Geol Eng. https://doi.org/10.1007/s10706-024-02953-8

Peck RB (1969) Advantages and limitations of the observational method in applied soil mechanics. Geotechnique 19(2):171–187. https://doi.org/10.1680/geot.1969.19.2.171

Prendergast LJ, Gavin K (2016) A comparison of initial stiffness formulations for small-strain soil–pile dynamic Winkler modelling. Soil Dyn Earthq Eng 81:27–41. https://doi.org/10.1016/j.soildyn.2015.11.006

Pujiastuti H, Rifai A, Adi AD, Fathani TF (2022) Single piles and pile groups capacity in unsaturated sandy clay based on laboratory test. ASEAN Eng J 12(1):165–171

Ramadan NO, Nasr AM, Azzam WR (2024) Experimental study on the behavior of single piles under combined torsional and vertical loads in contaminated sand. Geotech Geol Eng. https://doi.org/10.1007/s10706-024-02921-2

Shao W, Qin F, Shi D, Ali Soomro M (2024) Horizontal bearing characteristic and seismic fragility analysis of CFRP composite pipe piles subject to chloride corrosion. Comput Geotech 166:105977. https://doi.org/10.1016/j.compgeo.2023.105977

Siacara AT, Beck AT, Ji J (2024) Impact of random field simulations on FEM-based earth slope reliability. Geotech Geol Eng. https://doi.org/10.1007/s10706-024-02956-5

Venkatesan G, Murugan CA, Isac SJ, Gladson GJN (2022) Experimental investigation on load carrying capacity of hollow and composite pile materials in layered soil. Mater Today: Proc 65(9):3951–3958

Wang X, Li S, Li J (2022) Effect of pile arrangement on lateral response of group-pile foundation for offshore wind turbines in sand. Appl Ocean Res 124:103194

Wang X, Li S, Li J (2023a) Experimental and numerical study on lateral response of pile-group for offshore wind turbines in sand. Mar Georesour Geotechnol 41(5):524–543

Wang Z, Zhou H, Sheil B, Liu H, Wang C (2023b) Numerical investigation of the lateral response of pile groups in sand under local scour conditions. Comput Geotech 159:105435

Wen K, Wu X, Zhu B (2020) Numerical investigation on the lateral loading behaviour of tetrapod piled jacket foundations in medium dense sand. Appl Ocean Res 100:102193. https://doi.org/10.1016/j.apor.2020.102193

Wu WH, Prendergast LJ, Gavin K (2018) An iterative method to infer distributed mass and stiffness profiles for use in reference dynamic beam-Winkler models of foundation piles from frequency response functions. J Sound Vib 431:1–19. https://doi.org/10.1016/j.jsv.2018.05.049

Zhang X, Lu Y (2023) FEM analysis of wasted tire chip and sand as construction material for piles. Case Stud Construct Mater 18:1–11. https://doi.org/10.1016/j.cscm.2022.e01735

Zhang LM, McVay MC, Han SJ, Lai PW, Gardner R (2002) Effects of dead loads on the lateral response of battered pile groups. Canad Geotech J 39(3):561–575. https://doi.org/10.1139/t02-008

Zhang D, Cui H, Lei Z, Zhang X, Wang Z, Bai Y, Zhao H (2023) Soil arching effect of composite piles supporting foundation pits based on mechanical model and photoelastic experiment. Opt Lasers Eng 168:107644. https://doi.org/10.1016/j.optlaseng.2023.107644

Zyka K, Mohajerani A (2016) Composite piles: a review. Constr Build Mater 107:394–410. https://doi.org/10.1016/j.conbuildmat.2016.01.013

British Standards Institute. (2020). BS 8004:2015+A1:2020: Code of practice for foundations: British Standards Institute.

Castilla-Barbosa M, Ocampo-Terreros M, Rincón-Arango O (2024) A review of sand aging: mechanisms and impacts. *Geotech Geol Eng.*, 1673–1529. https://doi.org/10.1007/s10706-024-02923-0

Horeczko G (1995). *Marine application of recycled plastics*. Structures Congress XIII.

Pando MA. (2003). *A laboratory and field study of composite piles for bridge substructures.* PhD Thesis, Virginia Polytechnic Institute and State University.